Lipid biomarker distributions in Oligocene and Miocene sediments from the Ross Sea region, Antarctica

Duncan, Bella; McKay, Robert; Bendle, James; Naish, Timothy; Inglis, Gordon N.; Moossen, Heiko; Levy, Richard; Ventura, G. Todd; Lewis, Adam; Chamberlain, Beth; Walker, Carrie

[Link to publication on Research at Birmingham portal](#)

Lipid biomarker distributions in Oligocene and Miocene sediments from the Ross Sea region, Antarctica: Implications for use of biomarker proxies in glacially influenced settings

Bella Duncan[a], Robert McKay[a], James Bendle[b], Timothy Naish[a], Gordon N. Inglis[c], Heiko Moossen[b,d], Richard Levy[e], G. Todd Ventura[e,f], Adam Lewis[g], Beth Chamberlain[b,h], Carrie Walker[b,i].

[a]Antarctic Research Centre, Victoria University of Wellington, P.O. Box, Wellington 6012, New Zealand

[b]School of Geography, Earth and Environmental Sciences, University of Birmingham, Edgbaston, Birmingham, B15 2TT, UK

[c]Organic Geochemistry Unit, School of Chemistry and Cabot Institute, University of Bristol, Cantock's Close, Bristol BS8 1TS, UK

[d]Present address: Max Planck Institute for Biogeochemistry, P.O. Box 10 01 64, 07701 Jena, Germany

[e]Geological and Nuclear Sciences, P.O. Box 30-368, Lower Hutt 5040, New Zealand

[f]Present address: Department of Geology, Saint Mary's University, 923 Robie Street, Halifax, Nova Scotia, B3H 3C3, Canada

[g]North Dakota State University, Fargo, North Dakota, 58105, USA

[h]Present address: Department of Life Sciences, Imperial College London, Silwood Park Campus, Buckhurst Road, BioAscot, Berkshire, SL5 7PY, UK

[i]Present address: School of Environment, Earth and Ecosystem Sciences, The Open University, Milton Keynes, MK7 6AA, UK

Corresponding author: Bella Duncan, bella.duncan@vuw.ac.nz

Abstract

Biomarker-based climate proxies enable climate and environmental reconstructions for regions where other paleoclimatic approaches are unsuitable. The Antarctic Cenozoic record consists of widely varying lithologies, deposited in rapidly changing depositional settings, with large lateral variations. Previous sedimentological and microfossil studies indicate that the incorporation of reworked older material frequently occurs in these sediments, highlighting the need for an assessment of biomarker distribution across a range of depositional settings and ages to assess the role reworking may have on biomarker-based reconstructions. Here, we compare sedimentary facies with the distribution of n-alkanes and hopanoids within a terrestrial outcrop, two glaciomarine cores and a deep sea core, spanning the Late Oligocene to Miocene in the Ross Sea. Comparisons are also made with n-alkane distributions in Eocene glacial erratics and Mesozoic Beacon Supergroup sediments, which are both potential sources of reworked material. The dominant n-alkane chain length shifts from n-C_{29} to n-C_{27} between the Late Eocene and the Oligocene. This shift is likely due to changing plant community composition and the plastic response of n-alkanes to climate cooling. Samples from glaciofluvial environments onshore, and subglacial and ice-proximal environments offshore are more likely to display reworked n-alkane distributions, whereas, samples from lower-energy, lacustrine and ice-distal marine environments predominantly yield immature/contemporaneous n-alkanes. These findings emphasise that careful comparisons with sedimentological and paleontological indicators are essential when applying and interpreting n-alkane-based and other biomarker-based proxies in glacially-influenced settings.

Keywords: Paleoclimate, Antarctica, n-alkanes, biomarkers, hopanoids, reworking

1 Introduction

In Antarctic sediments, traditional microfossil-based methods of reconstructing climate can be challenging due to sparse distribution, low diversity of species, or poor preservation in sediments (i.e. Askin and Raine, 2000; Strong and Webb, 2000; Scherer et al., 2007). In contrast, biomarkers (molecular fossils preserved in the geological record) are relatively recalcitrant and have the potential to provide environmental proxy information when other methods are challenging or unsuitable. To date, only a few studies have employed biomarkers to investigate paleoclimate changes in Antarctica, with most of these conducted in offshore settings (i.e. Feakins et al., 2012; McKay et al., 2012; Pross et al., 2012; Bijl et al., 2013; Feakins et al., 2014; Levy et al., 2016; Rees-Owens et al., 2018). Such work is challenging because Cenozoic outcrops exposed in Antarctica are sparse, and are represented by relatively superficial and poorly-dated deposits of glacially derived tills, lacustrine and fluvial deposits, with occasional marine and glaciomarine sediments (Hambrey and Barrett, 1993; Marchant and Denton, 1996; Lewis et al., 2007; Lewis et al., 2008; Lewis and Ashworth, 2016). Sediments from drillcores on the continental margin are usually glaciomarine in origin and provide better-dated

2

67 records of cyclical fluctuations of the Antarctic Ice Sheets (Barrett, 1989; Naish et al., 2001, 2009).

68 However, the variable lithologies in these sediments and the nature of their deposition mean that

69 reworking of older sediments and associated fossil material is potentially a significant issue (e.g.,

70 Kemp and Barrett, 1975; Askin and Raine, 2000; Prebble et al., 2006a).
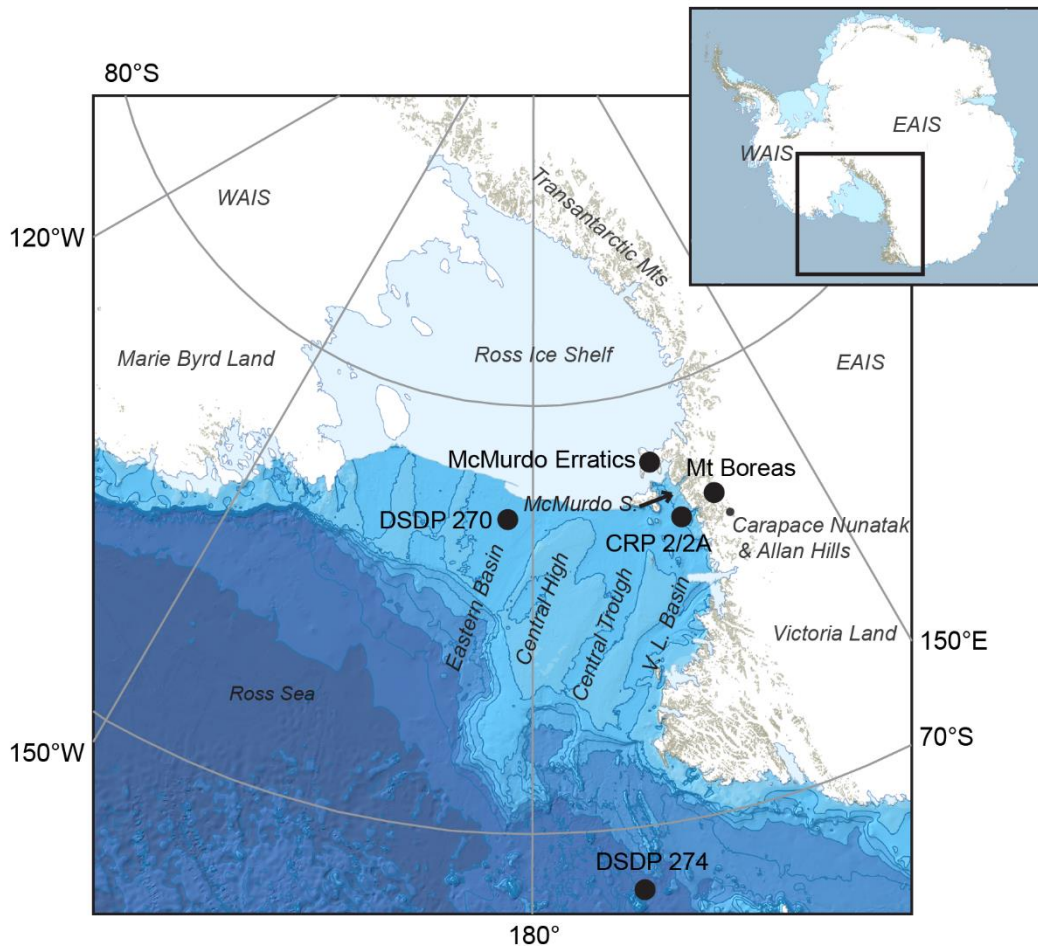
71

72 *Fig. 1: Location of sample sites in the Ross Sea region of Antarctica. WAIS: West Antarctic*

73 *Ice Sheet, EAIS: East Antarctic Ice sheet, DSDP: Deep Sea Drilling Project, CRP: Cape Roberts*

74 *Project, McMurdo S.: McMurdo Sound, V.L. Basin: Victoria Land Basin. Base map from*

75 *Quantarctica GIS package, Norwegian Polar Institute.*

76 Here, lipid biomarkers (*n*-alkanes and hopanoids) are used to investigate how organic matter

77 varies between different lithologies and depositional environments in the Ross Sea region of

78 Antarctica. Specifically, we aim to assess whether lipid biomarkers represent organic material sourced

79 from organisms living contemporaneously with sediment deposition, or older organic material which

80 has been reworked into the sediment. Knowledge of potential reworking is critical for using and

81 interpreting biomarker-based paleoenvironmental proxies in glacially-influenced settings. Localities

82 and sediment drill cores were chosen to survey a range of depositional environments that together

83 form a transect from high elevation terrestrial deposits to the deep sea (Fig. 1). These include; (i) A

3

84   Middle Miocene (~14 Ma) lacustrine/fluvial sequence from a small mountain glacier catchment at Mt

85   Boreas in the Transantarctic Mountains. (ii) A Late Oligocene/Early Miocene glaciomarine sequence

86   in the shallow marine Cape Roberts Project 2/2A drill core, sampling a coastal sediment catchment

87   from an East Antarctic Ice Sheet (EAIS) outlet glacier. (iii) A deeper water Late Oligocene/Early

88   Miocene glaciomarine sequence in DSDP Site 270 sampling sediment sourced from now submerged

89   islands and ice caps in the central continental shelf of the Ross Sea, West Antarctica. (iv) An Early

90   Miocene to Late Miocene marine sequence from DSDP Site 274 from the Western Ross Sea abyssal

91   plain, sampling a wide sediment source catchment from both East and West Antarctica.

92   *1.1 Geological setting*

93   The western Ross Sea region of Antarctica is bounded by the Transantarctic Mountains

94   (TAM), which were uplifted in the early Cenozoic, with the bulk of their exhumation occurring before

95   the early Oligocene (Fitzgerald, 1994; Smellie, 2001). The basement rocks of the TAM are dominated

96   by Archean to mid-Paleozoic metasediments and intrusives (Allibone et al., 1993a; Allibone et al.,

97   1993b; Goodge et al., 2002). The Devonian to Triassic Beacon Supergroup overlies this basement

98   (Barrett, 1981). Lithologies vary through the sequence, with interbedded sandstones, shales,

99   conglomerates and coals deposited in a paleoenvironmental setting moving from shallow marine to a

100   terrestrial system of lakes, braided rivers and alluvial plains (Barrett, 1981). Plant macrofossils and

101   palynomorphs are common throughout the Beacon Supergroup (Barrett, 1981). In the early Jurassic,

102   as the Gondwana super-continent began to separate, the Beacon Supergroup was intruded by the

103   Ferrar Dolerite, resulting in extensive low grade thermal metamorphism (Barrett, et al., 1986). The

104   Jurassic Ferrar Group contains extrusive volcanic rocks with fossiliferous sedimentary interbeds

105   containing terrestrial microfossil assemblages (e.g. Ribecai, 2007).

106   Scattered sedimentary outcrops and the basaltic McMurdo Volcanic Group form the Cenozoic

107   geology of the TAM (Marchant and Denton, 1996; Fielding et al., 2006; Martin et al, 2010). A

108   significant Cenozoic sedimentary unit distributed throughout the TAM is the Sirius Group, which

109   comprises glacial and non-glacial sediments with well-preserved fossil woody vegetation, leaf

110   material and peat beds, deposited in terrestrial and proximal marine environments (Hambrey and

111   Barrett, 1993; Francis and Hill, 1996; Barrett, 2013). Scattered Early Miocene to Holocene veneers of

112   glacial tills, colluvium and lacustrine deposits are dispersed through the TAM (Marchant and Denton,

113   1996; Lewis et al., 2007; Lewis et al., 2008; Lewis and Ashworth, 2016). Eocene to Pliocene glacial

114   erratics are found in the McMurdo region (Harwood and Levy, 2000). Much of what is currently

115   known about Cenozoic Antarctic climate is based on seismic stratigraphy and continental margin

116   drilling. Infill of sedimentary basins in the Ross Sea potentially began as early as the Late Cretaceous,

117   with sediment accumulation continuing through the Cenozoic (Cooper et al., 1987; De Santis et al.,

118   1995; Luyendyk et al., 2001; Decesari et al,, 2007; Wilson and Luyendyk, 2009). Continental margin

119　　drill cores from the Ross Sea contain successions of subglacial, glaciomarine and marine sediments

120　　reflecting the cyclical advance and retreat of the Antarctic Ice Sheets (i.e. Barrett, 1989; Naish et al.,

121　　2001; Naish et al., 2009; McKay et al., 2009; Levy et al., 2016).

122　　**2 Methods**

123　　*2.1 Site description*

124　　　　This work utilises samples from: (i) The McMurdo glacial erratics from the Mt Discovery and

125　　Minna Bluff region (Fig. 1), which yield marine and terrestrial micro- and macrofossils of mid-late

126　　Eocene age and are interpreted as being deposited in coastal-terrestrial and nearshore marine

127　　environments, under ice-free conditions (Harwood and Levy, 2000). (ii) Mid-Miocene terrestrial,

128　　fossil-bearing strata from Mt Boreas in the Olympus Range, which record the last known vestige of

129　　vegetation in the TAM before the Dry Valleys transitioned from wet- to cold-based glaciation at high

130　　altitudes (1,425 m) (Fig. 1) (Lewis et al., 2008). (iii) Oligocene/Early Miocene glaciomarine

131　　sediments obtained from the Cape Roberts Project core CRP-2/2A from the Victoria Land continental

132　　slope of Antarctica (Fig. 1) (Cape Roberts Science Team, 1999). (iv) A Late Oligocene to Early

133　　Miocene glaciomarine sequence of sediments from DSDP Site 270, drilled on the continental shelf in

134　　the central Ross Sea in 1973 and re-described in 2015 (Fig. 1) (The Shipboard Scientific Party, 1975a;

135　　Kraus, 2016). (v) An Early to Late Miocene succession of ice-distal diatom-rich silty clay sediments

136　　from DSDP 274 on the lower continental rise in the northwestern Ross Sea (68°59.81'S,

137　　173°25.64'W) (Fig. 1) (The Shipboard Scientific Party, 1975b). Figure 2 schematically describes the

138　　sampling sites and facies used in this study.

Facies 1: Siltstone, varying from diatom-rich to diatom-poor, and massive to laminated. Moss beds and fragments. Lacustrine environment of deposition.

Facies 2: Fine to coarse sandstone, with planar and trough crossbedding. Occasional gravel beds. Fluvial environment of deposition.

Facies 7: Muddy, fine- to coarse-grained graded sandstone. Deposited as turbidite beds in an ice distal marine environment with ice rafted sediment.

Facies 8: Mudstone. May contain sand and clasts. Varies between massive and stratified. Ice distal marine environment with sediment contribution from ice rafting. Stratified intervals may represent more ice-proximal periods.

☐ Sample site
1 Facies number
↓ Ice rafted debris
v Volcaniclastic sediment
〰 Density current

▢ Subglacial environment
▢ Ice-proximal environment
▢ Ice-distal environment
⊗ Bottom current
〰 Water current

Mt Boreas

Facies 3: Massive diamictite. Turbid, ice-proximal marine environment of deposition, close to an ice grounding line, but also possibly subglacial.

Facies 4: Stratified diamictite. Turbid, ice-proximal marine environment of deposition, in the grounding zone.

Facies 5: Interlaminated sandstone to mudstone. Cyclopels and cyclopsams deposited from turbid plumes in a tidally influenced ice-proximal marine setting.

Facies 6: Medium- to coarse-grained sandstone varying from massive to stratified. Marine environment of deposition close to a glaciofluvial/ glaciodeltaic outwash system.

Facies 9: Volcaniclastic lapillistones. Volcanic sediment deposited in a marine environment.

CRP 2/2A

DSDP 270

Facies 10: Diatom-rich mudstone. Deep marine environment of deposition under a weak bottom current regime, including turbidite beds, reduced ice-rafting component.

Facies 11: Diatom mudstone with clasts and manganese nodules. Deep marine environment of deposition under a strong bottom current regime, with coarse sediment contribution from ice rafting concentrated by winnowing.

DSDP 274

139

140   Fig. 2. Schematic representation of Oligocene and Miocene environments of deposition in the Ross Sea Region, and their associated sedimentary

141   facies. Sample sites are placed in their representative depositional setting.

142

2.2 Bulk analysis

Unless already desiccated, samples were freeze dried for 48 h prior to sample work up. All samples were homogenised to a powder using a Retsch 200 mixer mill.

Pyrolysis measurements for total organic carbon (TOC) were made using a Weatherford laboratories Source Rock Analyzer at GNS Science on ~100 mg of powdered sediment. The pyrolysis program was set with the sample crucible entering the pyrolysis oven where it was held isothermal at 300 °C for 3 mins under a continuous stream of He carrier gas using a 100 ml/min flow rate. This was followed by a 25 °C/min ramp to 650 °C. The S1 and S2 signal intensities were recorded with a FID operated under a 65 ml/min stream of H_2 gas and 300 ml/min air. The pyrolysis cycle was then followed by an oxidation cycle performed at 630 °C for 20 mins during which time the oven and crucible were flushed with dry air at 250 ml/min. The generated carbon monoxide and carbon dioxide gases were measured by the instrument's IR cells. All sample sequences were run with three IFP 160000 analytical standard replicates (from Vinci Technologies, Institut Français du Pétrole) placed at the beginning, middle and end of each sample sequence.

2.3 Lipid biomarker analyses

Organic geochemical work-up, gas chromatograph (GC)-flame ionization detector (FID) and GC-Mass Spectrometer (MS) analyses was performed in the Birmingham Molecular Climatology Laboratory (BMC), University of Birmingham. Lipids were extracted from ~10-15 g of homogenised sediment by ultrasonic extraction using dichloromethane (DCM):methanol (3:1). The total lipid extract was fractionated by silica gel chromatography using *n*-hexane, *n*-hexane:DCM (2:1), DCM, and methanol to produce four separate fractions, the first of which contained the aliphatic saturated and unsaturated hydrocarbons (e.g. *n*-alkanes, steranes and hopanes). Procedural blanks were also analysed to ensure the absence of laboratory contaminants.

The aliphatic hydrocarbon fractions were analysed on an Agilent 7890B series GC, equipped with a 7639ALS autosampler, a BP5-MS column (SGE Analytical Science, 60 m × 0.32 mm × 0.25 μm) and an FID, using hydrogen (H_2) as a carrier gas. Compound separation was achieved by using the following temperature program: the oven was held at 70 °C for 1 min, then heated to 120 °C at 30 °C/min, and then to 320 °C with 3 °C/min, where it was held for 20 mins. GC-Mass spectrometry (GC-MS) was performed using an Agilent 7890B GC, coupled to an Agilent 5977A Mass Selective Detector (MSD). The same capillary column and temperature program was used throughout the analyses for consistent compound separation. Helium (He) was used as a carrier gas. Samples were bracketed with an external standard containing known abundances of certain *n*-alkanes to allow identification and quantification of *n*-alkanes (average standard deviation of ± 7.6%). *n*-Alkane peaks

176   were integrated in Agilent OpenLAB Data Analysis Version A.01.01 - Build 1.93.0. Relationships

177   between n-alkane indices were investigated using Pearson's correlation coefficients and assessed as

178   statistically significant when $p<0.05$. Hopanes and hopenes were identified based upon published

179   spectra, characteristic mass fragments and retention times (e.g. Rohmer et al., 1984; Sessions et al.,

180   2013; Inglis et al., 2018) and integrated using GC-MS.

181   *2.4 Biomarker indices*

182   n-Alkanes of specific carbon chain lengths are known to be derived from discrete biological

183   sources. Algae and some photosynthetic bacteria typically produce dominantly n-C_{17}, with lesser

184   amounts of n-C_{15} and n-C_{19} (Clark and Blumer, 1967; Han and Calvin, 1969; Cranwell et al., 1987).

185   Other species of bacteria, including non-photosynthetic bacteria often demonstrate an even carbon

186   number preference between n-C_{12} and n-C_{22}, commonly with high n-C_{16} and n-C_{18} (Han and Calvin,

187   1969; Grimalt and Albaigés, 1987). Non-emergent aquatic plants and *Sphagnum* mosses show

188   enhanced production of n-C_{23} and n-C_{25} (Baas et al., 2000; Ficken et al., 2000; Pancost et al., 2002;

189   Bingham et al., 2010). Long chain n-alkanes (n-C_{25} and higher), usually with a high odd-over-even

190   predominance, are most abundant in the epicuticular waxes on leaves and stems of terrestrial higher

191   plants (Eglinton and Hamilton, 1963). n-Alkanes are also derived from the early diagenetic alteration

192   of saturated and unsaturated aliphatic alcohols, ketones, esters, and di- or triterpenic acids (i.e. Tissot

193   and Welte, 1984; Meyers and Ishiwatari 1993). Once deposited, n-alkanes may undergo microbial or

194   geochemical alteration, modifying their distributions (Grimalt et al., 1985).

195   The source and maturity of higher molecular weight n-alkanes can be characterised by their

196   carbon preference index (CPI):

197    $$CPI = \frac{1}{2}\left(\left(\frac{\Sigma_{odd}(n-C_{25-33})}{\Sigma_{even}(n-C_{24-32})}\right) + \left(\frac{\Sigma_{odd}(n-C_{25-33})}{\Sigma_{even}(n-C_{26-34})}\right)\right) \qquad (1)$$

198   Most modern sediments with terrestrially sourced organic matter have an odd-over-even

199   predominance of long chained n-alkanes (n-C_{25} to n-C_{34}) and CPI values >1 (Bray and Evans, 1961;

200   Eglinton and Hamilton, 1963). A survey of modern leaf wax material demonstrates that a CPI of >1-2

201   is a reasonable threshold value indicative of relatively unmodified terrestrial plant material (Bush and

202   McInerney, 2013). Sediments containing CPI values of <1 usually indicate either exposure to elevated

203   burial temperatures great enough to cause hydrocarbon cracking, or an input of organic matter that has

204   been altered by diagenetic or catagenetic processes (Bray and Evans, 1961). Some sediments will also

205   display an unresolved complex mixture (UCM), represented by a hump in the baseline of a gas

206   chromatogram due to the co-elution of unresolved compounds (Gough and Rowland, 1990; Gough et

207   al., 1992). UCMs can be especially prominent in biodegraded petroleums, in which microbial

208   degradation of the more abundant aliphatic components leads to increased concentrations of the more

209   recalcitrant, branched and cyclic compounds (Gough and Rowland, 1990; Gough et al., 1992). In

210 recent sediments, *n*-alkanes have a lower susceptibility to microbial degradation than most other types

211 of organic matter as they lack functional groups, but studies on peat and lake sediments suggest that

212 microbial degradation does occur (Meyers and Ishiwatari, 1993; Lehtonen and Ketola, 1993). Shorter

213 chain lengths appear more degradable than longer chain lengths, and microbial degradation can result

214 in a decrease in CPI (Meyers and Ishiwatari, 1993; Lehtonen and Ketola, 1993).

215   Average chain length (ACL) indicates the dominant *n*-alkane in a given carbon number range

216 (Poynter et al., 1989; Schefuß et al., 2003):

217 $$ACL = \frac{\Sigma(C_{odd\,25-33} \cdot x_{odd\,25-33})}{(x_{odd\,25-33})}$$ (2)

218   Where $C_{odd\,25-33}$ represents the carbon number of the odd chain length *n*-alkanes, and $x_{odd\,25-33}$

219 represents the concentrations of the odd *n*-alkanes in the sample. ACL is influenced by a number of

220 factors. Higher ACLs are typical of warmer, tropical regions, whilst lower ACLs are more commonly

221 observed from cooler, temperate regions, indicating that ACL could be related to air temperature

222 (Gagosian and Peltzer, 1986; Poynter et al., 1989; Dodd and Afzal-Rafii, 2000; Kawamura et al.,

223 2003; Bendle et al., 2007; Vogts et al., 2009; Bush and McInerney, 2015). Other studies have

224 suggested that aridity has a strong control on ACL, with the synthesis of longer *n*-alkanes in more arid

225 environments providing plants with a more efficient wax coating to restrict water loss (Dodd et al.,

226 1998; Dodd and Afzal-Rafii, 2000; Schefuß et al., 2003; Calvo et al., 2004; Zhou et al., 2005;

227 Moossen et al., 2015). ACL is also strongly controlled by the contributing vegetation, with large inter-

228 and intra-species variation in *n*-alkane distributions (i.e. Vogts et al., 2009; Bush and McInerney,

229 2013; Feakins et al., 2016). Variation in average chain length through time therefore reflects the

230 interplay of two key factors: climate-driven plastic response of *n*-alkanes to temperature and/or aridity

231 within a plant community; or changes to the composition of the plant community, often in response to

232 climate (Bush and McInerney, 2013).

233   Hopanes and hopenes are C_{27} to C_{35} pentacyclic triterpenoids derived from a wide range of

234 bacteria (Rohmer et al., 1984; Talbot and Farrimond, 2007). Hopanes are ubiquitous across a variety

235 of depositional settings, and in both modern and ancient sediments (Ourisson and Albrecht, 1992). In

236 modern sediments, hopanes are mostly present in the biological 17β,21β(H) configuration (although

237 there are exceptions; see Inglis et al., 2018). In sediments, with increasing diagenesis, hopanes

238 undergo stereochemical transformations and the biologically-derived 17β,21β(H)-hopanoid is

239 transformed into the more thermally stable 17β,21α(H) and 17α,21β(H)-stereoisomers (Mackenzie et

240 al., 1980; Peters and Moldowan, 1991). With increasing maturation, extended hopanoids ($>C_{30}$) also

241 undergo isomerisation at the C-22 position. As such, hopanoids are frequently used to reconstruct

242 thermal maturity (Mackenzie et al., 1980; Seifert and Moldowan, 1980; Peters and Moldowan, 1991;

243 Farrimond et al., 1998), where decreasing ββ/(αβ+βα+ββ) indices and increasing 22S/(22R + 22S)

244 values indicate increasing thermal maturity. The ratio of C_{27} 18α(H)-trisnorhopane II (Ts) to C_{27}

245   17α(H)-trisnorhopane (Tm) is also commonly used as a maturity parameter, as Tm is less stable

246   during catagenesis than Ts (Seifert and Moldowan, 1978).

247   **3 Results**

248   *3.1 Facies compilation*

249   In order to compare results between sites, an internally consistent facies scheme was

250   developed based on published facies descriptions for each sample site (Fig. 2). The McMurdo erratics

251   were not included, as the context and relationship between these samples is uncertain. Instead these

252   samples were labelled by lithofacies as described by Levy and Harwood (2000) (Supplementary table

253   1). Samples from Mt Boreas were assigned facies based on descriptions from Lewis et al. (2008).

254   Facies for CRP 2/2A were developed based on descriptions of Fielding et al. (2000). Facies for DSDP

255   270 were assigned using descriptions of Kraus (2016), and based on previous models of glaciomarine

256   facies successions (Fielding et al, 2000; Powell and Cooper, 2002; McKay et al., 2009). For DSDP

257   274, facies were determined by using interpretations from The Shipboard Scientific Party (1975b),

258   Frakes (1975) and Whittaker and Müller (2006).

259   *3.2 McMurdo erratics*

260   Six Mid- Late Eocene sediment samples from the McMurdo erratics suite were analysed for

261   *n*-alkanes, sourced from a range of lithofacies (Levy and Harwood, 2000) (Supplementary table 1).

262   Three of the samples (E214, MB245 and E215) are dominated by the n-C_{17} to n-C_{20} short chained n-

263   alkanes underlain by a UCM (Fig. 3). Samples D1, E219 and MTD95 have bimodal profiles,

264   dominated by ~n-C_{20} to n-C_{23} underlain by small a UCM, and a series of longer n-alkanes with a

265   mode at ~n-C_{29} (Fig. 3). In all samples, n-C_{29} is the dominant long-chained n-alkane, in contrast to

266   younger strata investigated in this study usually dominated by n-C_{27}. The ratio between these two

267   chain lengths has been described at all sites to investigate its variance at other localities. The CPI from

268   the McMurdo Erratics ranges from 1.8 to 5.5 (avg. 2.8). ACL varies from 27.9 to 28.7 (avg. 28.2),

269   whilst the ratio of the n-C_{29} n-alkane to n-C_{27} ranges from 1.01 to 1.64 (avg. 1.26). The erratics

270   contain total abundances of n-alkanes ranging from 83 μg/gTOC to 1579 μg/gTOC, at an average of
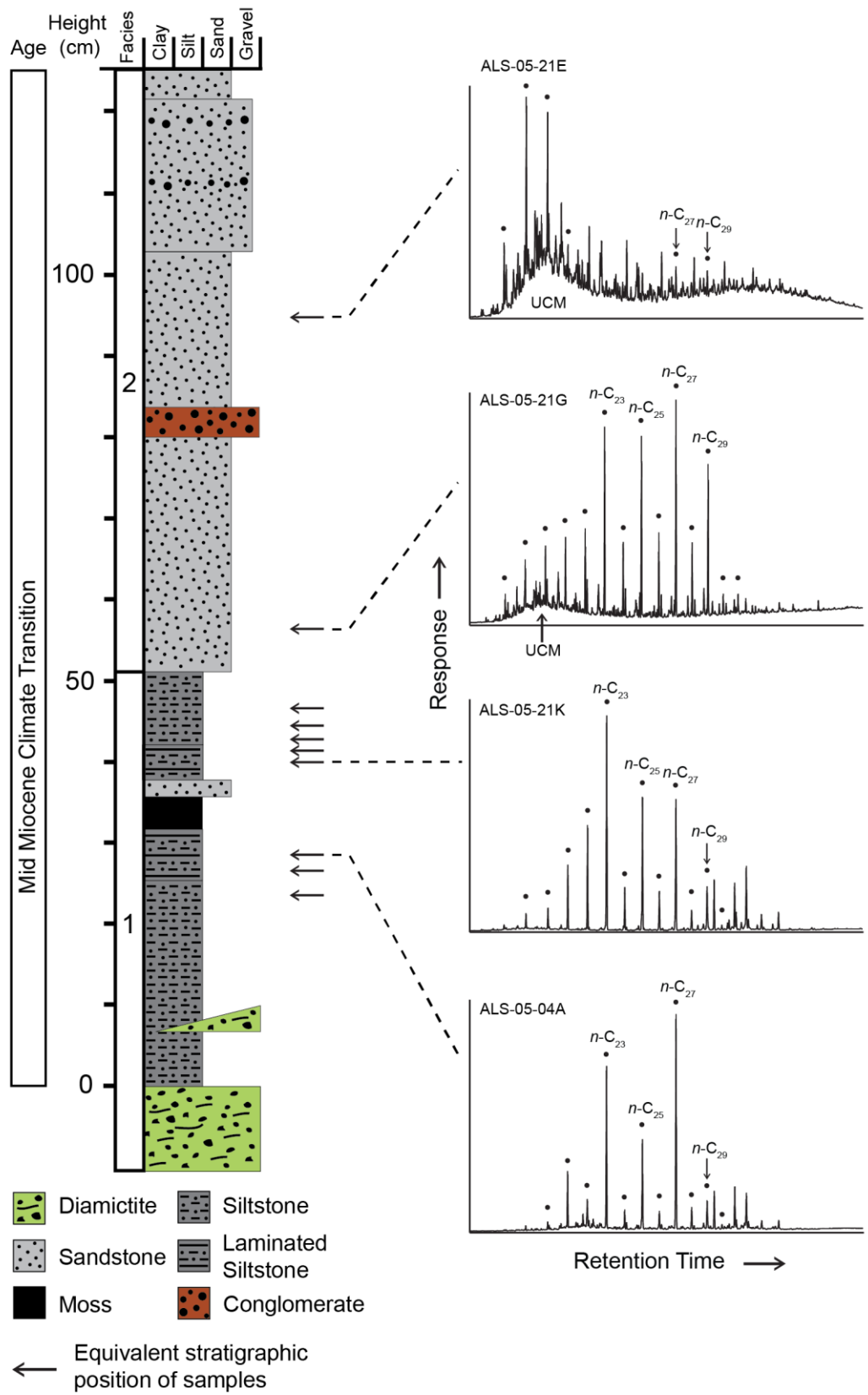
271   406 μg/gTOC.
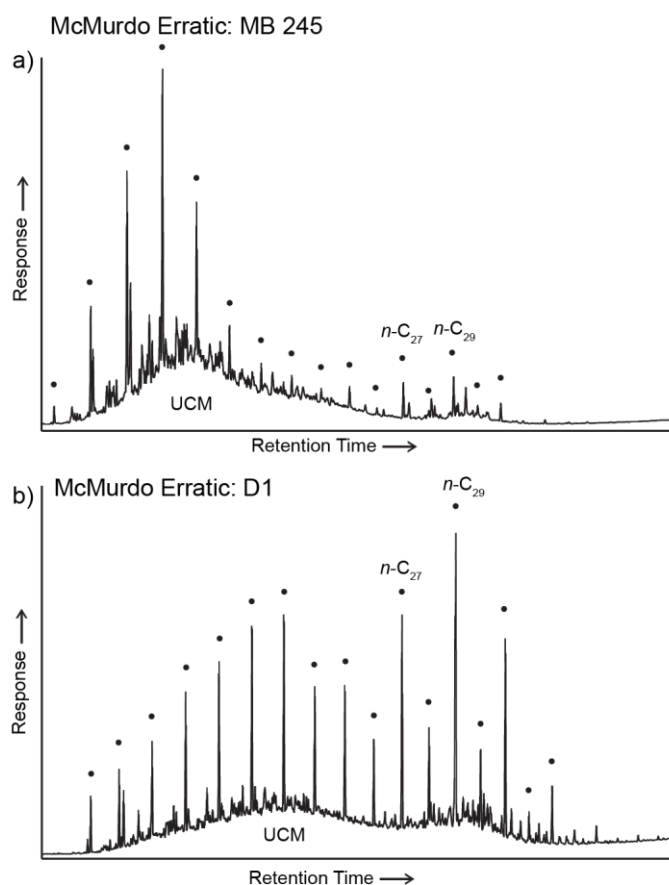
Fig. 3. Representative GC-FID-chromatograms of two samples of the McMurdo erratics. Filled circles above peaks indicate n-alkanes, with the n-C_{27} and n-C_{29} labelled. UCM: unresolved complex mixture.

3.3 Mt Boreas

12 sediment samples from Mt Boreas were analysed for *n*-alkanes (Supplementary table 1) Samples from Mt Boreas are typically dominated by long chained *n*-alkanes, particularly *n*-C_{23}, *n*-C_{25} and *n*-C_{27} (Fig. 4). Some samples display small UCMs, usually underlying ~*n*-C_{19} to *n*-C_{20}. Samples were collected from three different sites within a topographic depression which held a small alpine line, from units that are correlatable to the stratigraphic column shown in Figure 4 (Lewis et al., 2008). The total abundance of *n*-alkanes at these sites ranges between 4.5 µg/gTOC to 762 µg/gTOC, at an average of 206.5 µg/gTOC. The CPI of the long-chained *n*-alkanes ranges from 1.7 to 5.9 (avg. 3.4), whilst ACL varies from 26.2 to 27.4 (avg. 26.9). The ratio of the *n*-C_{29} *n*-alkane to *n*-C_{27} varies from 0.15-0.97 (avg. 0.55), indicating that the *n*-C_{27} dominates the *n*-C_{29} in all samples from these sites (Supplementary table 1).

11

288   *Fig. 4. Stratigraphic column from a site at Mt Boreas (after Lewis et al., 2008) with the*

289   *equivalent stratigraphic positions of representative GC-FID-chromatograms of samples. Filled*

290   *circles above peaks indicate n-alkanes, with the n-C_{27} and n-C_{29} labelled. Facies numbers are*

291   *described in Fig. 2. UCM: unresolved complex mixture.*

292   Pearson's correlation coefficients were estimated for each *n*-alkane variable compared to

293   other *n*-alkane variables from these sites. Only two variables demonstrate a statistically significant

294   correlation to each other; the ratio of *n*-C_{29}/*n*-C_{27} typically decreases with increasing CPI ($r = 0.711$, p

295    $= 0.0096$) (Fig. 5). Samples from fluvial Facies 2 typically display lower CPI, and higher ACL and *n*-

296   C_{29}/*n*-C_{27} values than those from lacustrine Facies 1, although it is noted that the Facies 2 is only

297   represented by two samples (Fig. 6). Both fluvial and lacustrine samples show similar average total
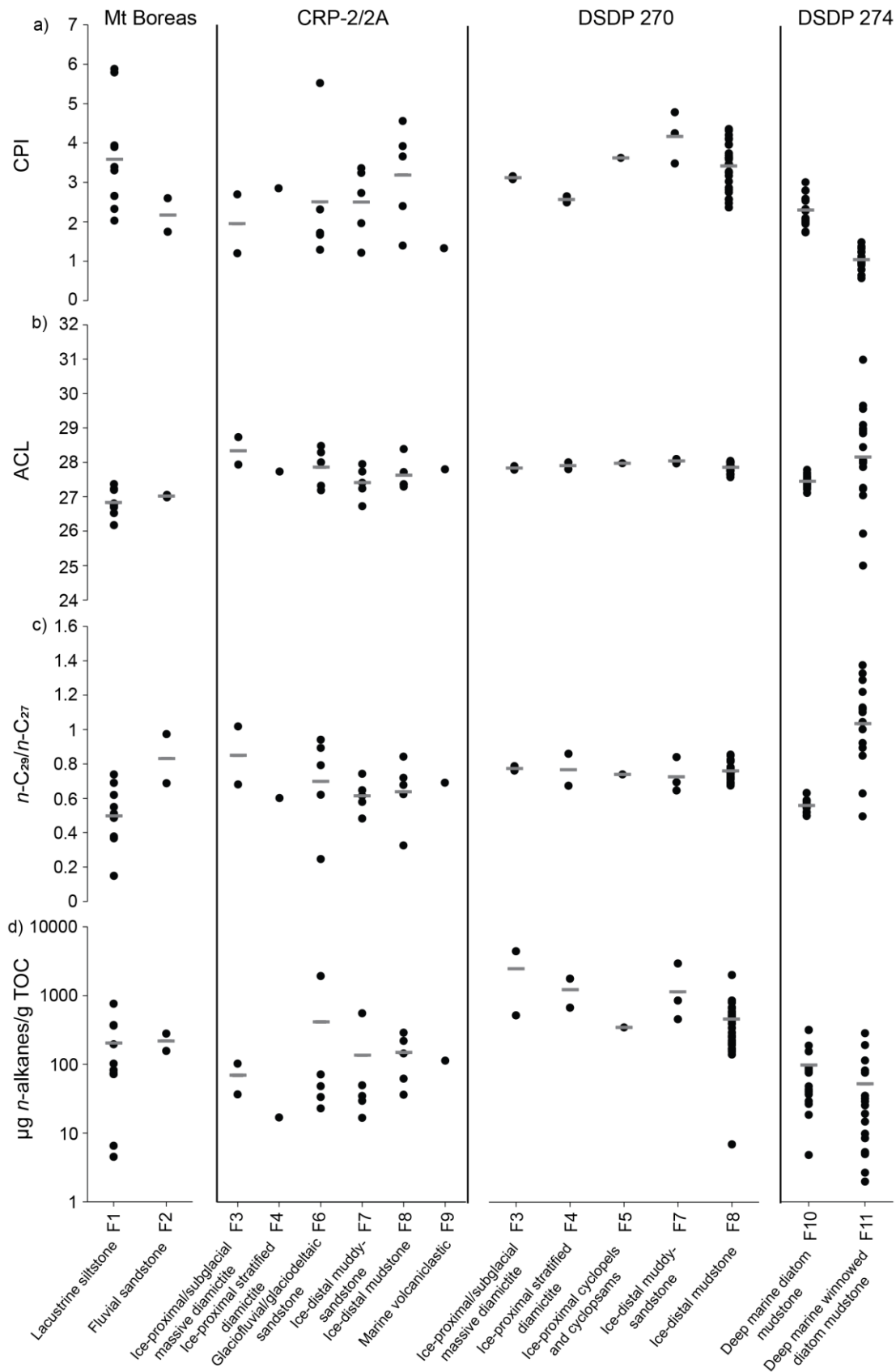
298   abundances of *n*-alkanes.
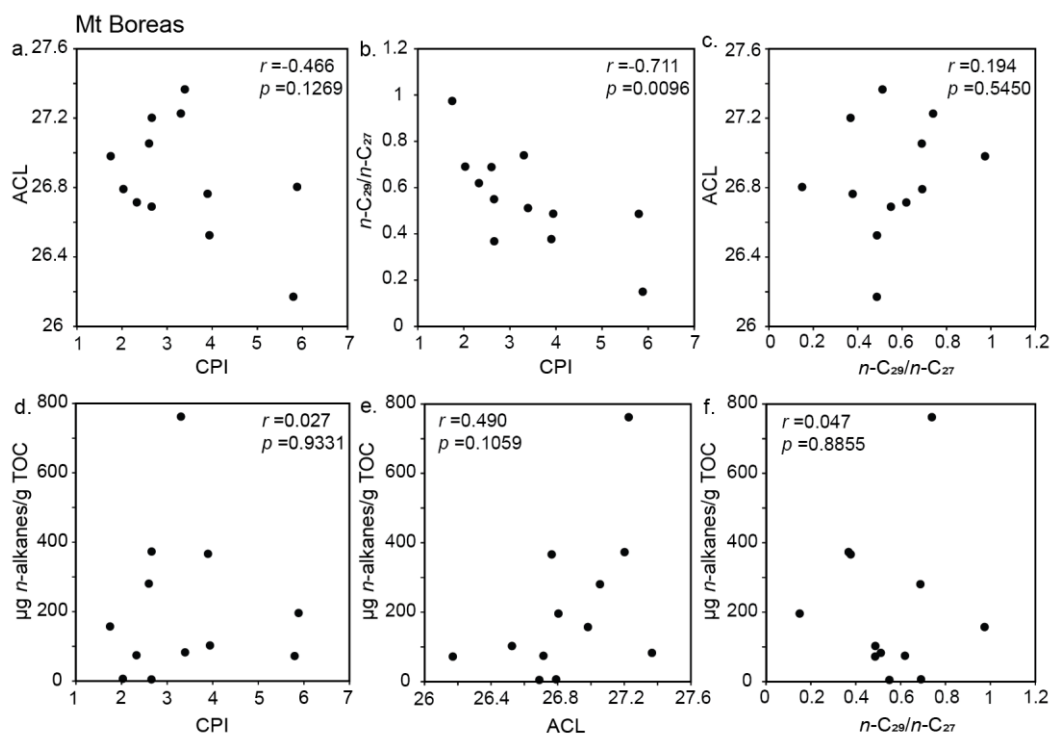
300   *Fig. 5. Scatter plots of samples from Mt Boreas; a) CPI and ACL; b) CPI and n-C_{29}/n-C_{27}; c)*

301   *n-C_{29}/n-C_{27} and ACL; d) CPI and the total abundance of n-alkanes (µg n-alkanes/g TOC); e) ACL and*

302   *the total abundance of n-alkanes (µg n-alkanes/g TOC) and f) n-C_{29}/n-C_{27} and the total abundance of*

303   *n-alkanes (µg n-alkanes/g TOC).*

304   Three samples representing typical *n*-alkane distributions from the site were also analysed for

305   additional biomarkers (Supplementary table 2). In two samples (ALS-05-21N and ALS-05-04C),

306   hopanoids were abundant and the distribution was dominated by 17β(H)-trisnorhopane (C_{27}) and

307   17β,21β(H)-norhopane (C_{29}). Both samples are characterised by high ββ/(αβ+βα+ββ) ratios (0.82 to

308   0.86) and indicate low thermal maturity. Within sample ALS-05 21O, hopanoids were weak and the

309   distribution was dominated by thermally-mature C_{27} to C_{35} hopanes. This sample was characterised by

a low ββ/(αβ+βα+ββ) ratio (0.07) and high C22S/C22R+C22S ratio (0.58) and therefore indicate high

thermal maturity.

Fig. 6: Distributions of n-alkane variables across different facies from Mt Boreas, CRP-2/2A,

314 *DSDP 270 and DSDP 274; a) CPI, b) ACL, c) n-C_{29}/n-C_{27} and d) the total abundance of n-alkanes*

315 *(μg n-alkanes/g TOC). Grey bars represent average values for each facies. Description of facies in*

316 *Fig. 2.*

317 *3.4 Cape Roberts Project 2/2A*

318   Long chained *n*-alkanes typically dominate samples from CRP 2/2A (Fig. 7). The *n*-C_{23}, *n*-C_{25}

319 and *n*-C_{27} are usually the most abundant homologs, with *n*-C_{27} often the most prominent of these. In

320 some samples *n*-alkanes elute with a UCM, which is usually centred between *n*-C_{19} and *n*-C_{23}. The

321 total abundance of *n*-alkanes is highly variable from sample to sample, ranging from 16.6 μg/gTOC to

322 1893.0 μg/gTOC, averaging 197.6 μg/gTOC. CPI also varies over a wide range, from 1.2-5.5 (avg.

323 2.6), whilst ACL ranges from 26.7-28.7 (avg. 27.7). The ratio of the *n*-C_{29} *n*-alkane to *n*-C_{27} varies

324 from 0.25-1.02 (avg. 0.67) (Supplementary table 1).

325   Pearson's correlation coefficient estimations show statistically significant correlations

326 between several *n*-alkane variables. The strongest correlations exist between CPI and *n*-C_{29}/*n*-C_{27} ($r =$

327 0.837, $p < 0.0001$) and ACL and *n*-C_{29}/*n*-C_{27} ($r = 0.777$, $p < 0.0001$), with a weaker correlation

328 between CPI and ACL ($r = 0.580$, $p = 0.0091$). Figure 8 shows that at both high and low values of

329 CPI and *n*-C_{29}/*n*-C_{27}, the total abundance of *n*-alkanes increases, with weak correlations between these

330 variables ($r = 0.516$, $p = 0.0238$ and $r = 0.520$, $p = 0.0225$, respectively). Most facies contain a range

331 of both high and low values of CPI, with the highest average CPI in the low-energy marine mudstones

332 of facies 8 (Fig. 6). Facies 6, 7 and 8 also have broad ranges of ACL and *n*-C_{29}/*n*-C_{27}, with the lowest

333 average ACL and *n*-C_{29}/*n*-C_{27} in the poorly sorted sandstones of facies 7, while facies 3, consisting of

334 massive diamictites, has the highest average ACL and *n*-C_{29}/*n*-C_{27}. Two samples containing a much

335 higher concentration of *n*-alkanes than other samples in the facies skew the averages for facies 6 and

336 7. Without these outliers, facies 8 contains the highest average total abundance of *n*-alkanes.

337   Additional biomarkers were investigated in two samples, with a range of C_{27}–C_{32} hopanes and

338 C_{27}–C_{30} hopenes were present (Supplementary table 2). The dominant compound was 17β,21β(H)-

339 bishomohopane (C_{32}) or 17α,21β(H)-hopane (C_{30}) and samples were characterised by low-to-

340 moderate $\beta\beta$/($\alpha\beta$+$\beta\alpha$+$\beta\beta$) ratios (0.45 to 0.65). As such, these samples are characterised by relatively
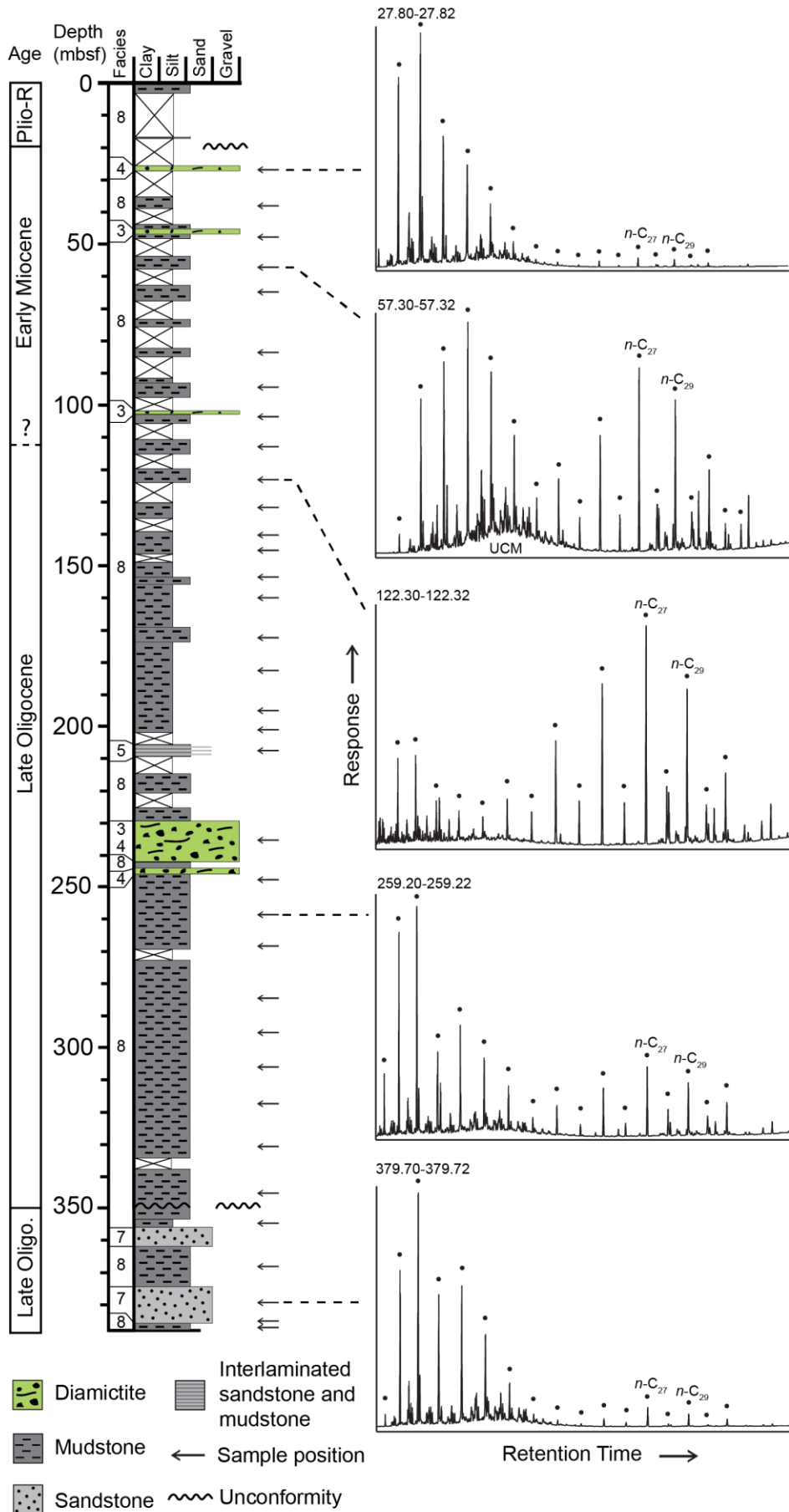
341 low thermal maturity.
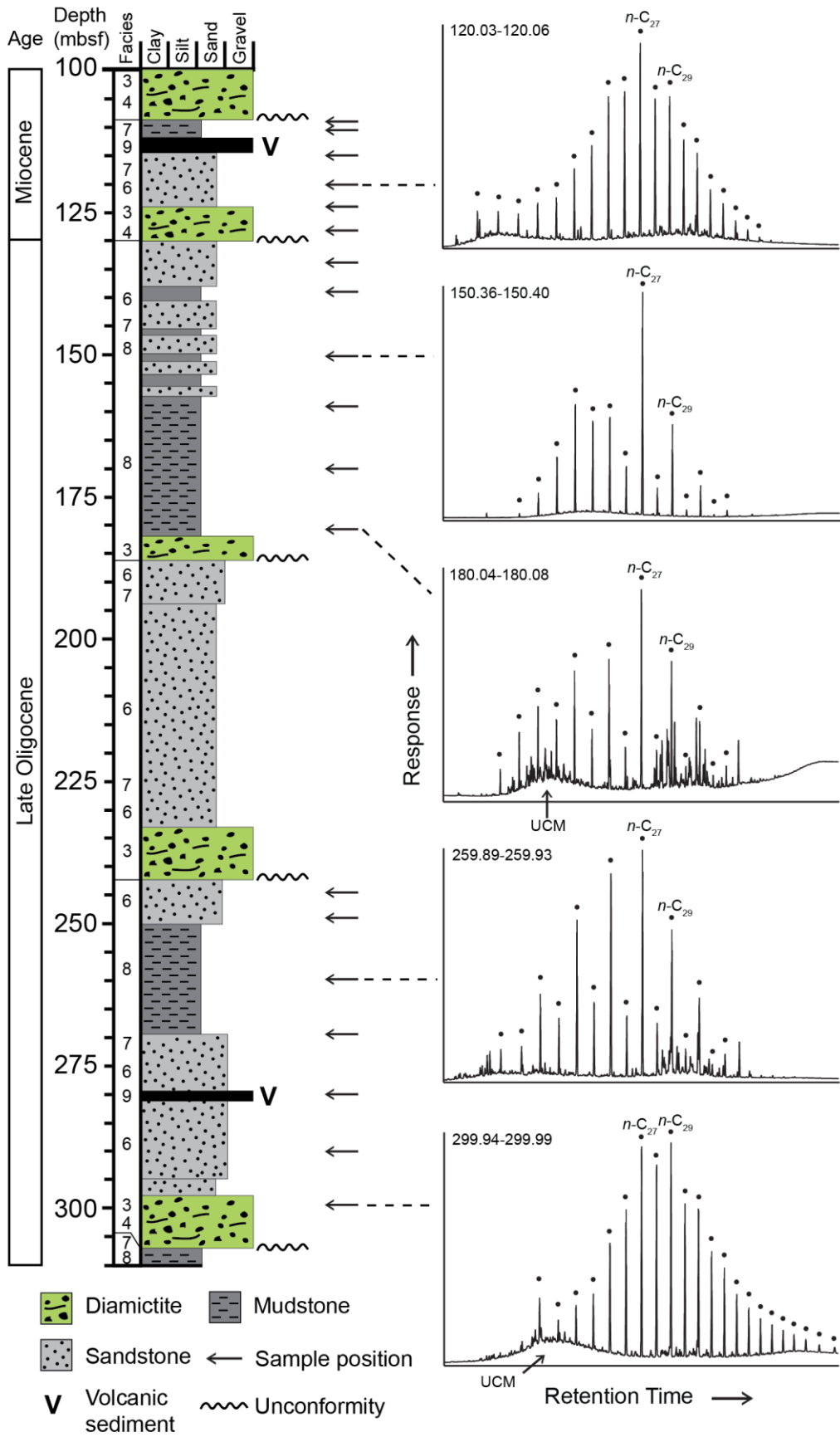
343   *Fig. 7. Stratigraphic column from CRP 2/2A with the stratigraphic positions of representative*

344   *GC-FID-chromatograms of samples. Filled circles above peaks indicate n-alkanes, with the n-C_{27} and*

345   *n-C_{29} labelled. Simplified facies groupings are labelled, and are described in table 1. UCM:*

346   *unresolved complex mixture.*
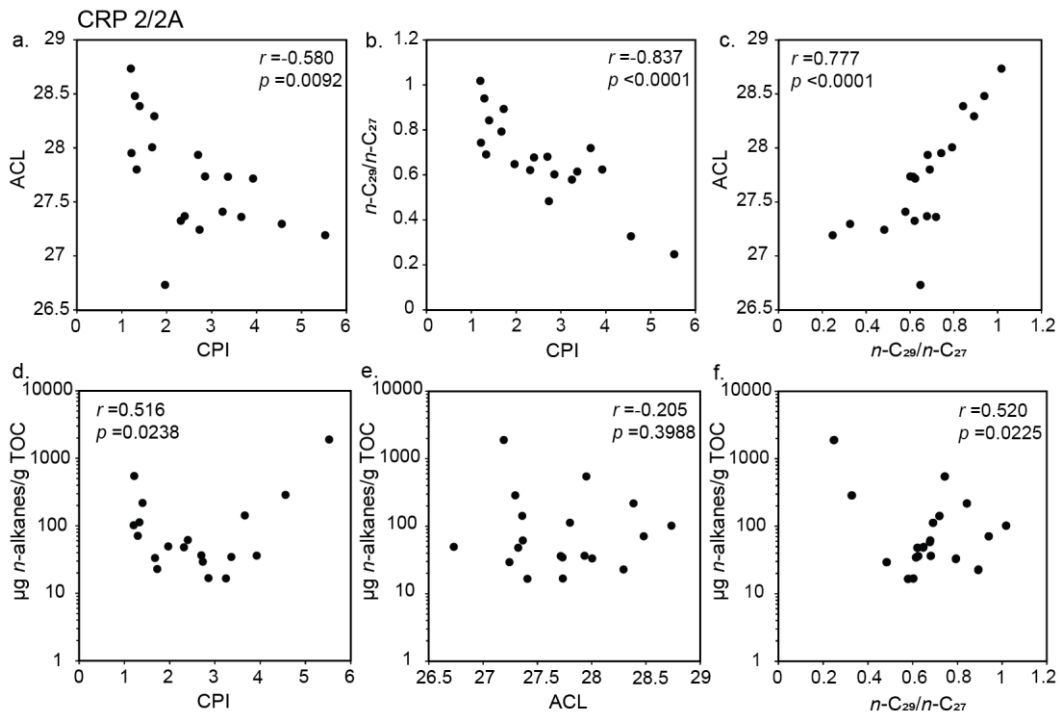
348   *Fig. 8. Scatter plots of samples from CRP 2/2A; a) CPI and ACL; b) CPI and n-C_{29}/n-C_{27}; c)*

349   *n-C_{29}/n-C_{27} and ACL; d) CPI and the total abundance of n-alkanes (μg n-alkanes/g TOC); e) ACL and*

350   *the total abundance of n-alkanes (μg n-alkanes/g TOC) and f) n-C_{29}/n-C_{27} and the total abundance of*

351   *n-alkanes (μg n-alkanes/g TOC).*

3.4 DSDP 270

353   Samples from DSDP 270 typically display bimodal *n*-alkane distributions with a peak at n-C_{17}

354   or n-C_{19} and another peak n-C_{27} (Fig. 9). Shorter chained *n*-alkanes (> n-C_{20}) are usually more

355   abundant than the long chained homologs, and in four samples from the lowest sampled section of the

356   core, long chained *n*-alkanes were not detected. Some samples display a small UCM underlying ~n-

357   C_{20} and n-C_{21}. CPI of the long chained *n*-alkanes ranges from 2.4-4.8 (avg. 3.4). ACL varies from

358   27.6-28.1 (avg. 27.9), whilst the ratio of n-C_{29} to n-C_{27} ranges from 0.65-0.86 (avg. 0.76). The

359   samples have an average total abundance of *n*-alkanes of 680.92 μg/gTOC (Supplementary table 1).

17

Fig. 9. Stratigraphic column from DSDP 270 with the stratigraphic positions of

362 *representative GC-FID-chromatograms of samples. Filled circles above peaks indicate n-alkanes,*

363 *with the n-C_{27} and n-C_{29} labelled. Simplified facies groupings are labelled, and are described in table*

364 *1. UCM: unresolved complex mixture.*

365   Pearson's correlation coefficients show no particularly strong correlations between *n*-alkane

366 variables. Increasing *n*-C_{29}/*n*-C_{27} with decreasing CPI is very weakly correlated ($r = 0.391$, $p =$

367 0.0221), with a slightly stronger correlation existing between decreasing *n*-C_{29}/*n*-C_{27} with decreasing

368 ACL ($r = 0.533$, $p = 0.0012$) (Fig. 10). When grouped by facies, facies 7 demonstrates the highest

369 average CPI, and facies 4 contains the lowest average CPI (Fig. 6). Facies 7 shows the highest

370 average ACL and lowest average *n*-C_{29}/*n*-C_{27}, but most facies display similar ACL and *n*-C_{29}/*n*-C_{27}

371 values. Most facies also contain a similar total abundance of *n*-alkanes, with the highest average

372 abundance in facies 3.

373   Two samples with representative *n*-alkane distributions were analysed for additional

374 biomarkers (Supplementary table 2). Samples contained a range of C_{27}–C_{32} hopanes and C_{27}–

375 C_{30} hopenes. The dominant compounds were 17β(H)-trisnorhopane (C_{27}), 17α,21β(H)-hopane

376 (C30),17β,21β(H)-homohopane (C_{31}). Both samples were characterised by high ββ/(αβ+βα+ββ) ratios

377 (0.69 to 1.00) and indicate low thermal maturity.

379 *Fig. 10. Scatter plots of samples from DSDP 270; a) CPI and ACL; b) CPI and n-C_{29}/n-C_{27};*

380 *c) n-C_{29}/n-C_{27} and ACL; d) CPI and the total abundance of n-alkanes (µg n-alkanes/g TOC); e) ACL*

381   *and the total abundance of n-alkanes (µg n-alkanes/g TOC) and f) n-C$_{29}$/n-C$_{27}$ and the total*

382   *abundance of n-alkanes (µg n-alkanes/g TOC).*
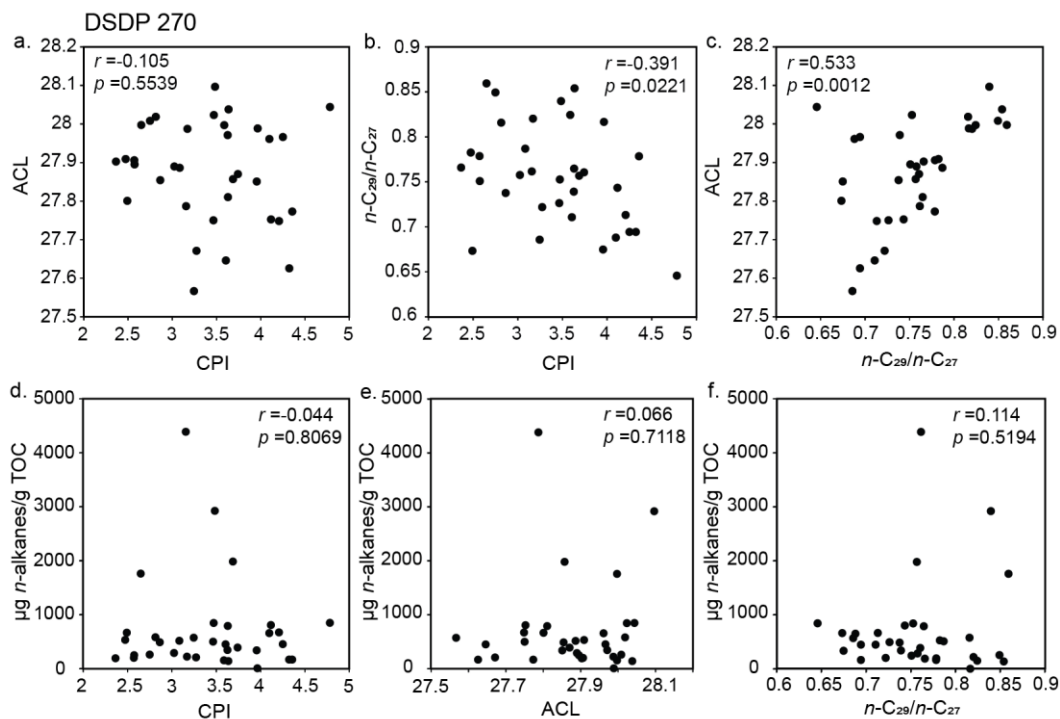
383   *3.5 DSDP 274*

384   Samples taken from above 115m had variable, or even absent, quantities of *n*-alkanes (Fig.

385   11). Samples usually contained significant UCMs, which typically dominated the signal, and *n*-

386   alkanes did not display a common dominant *n*-alkane. Samples below 115m were usually bimodal in

387   distribution, with a dominant *n*-alkane peak around *n*-C$_{19}$, *n*-C$_{20}$ or *n*-C$_{21}$, underlain by a UCM, and

388   another peak centred at *n*-C$_{27}$. CPI ranges from 0.6 to 3.0 (avg. 1.6), whilst ACL ranges from 25 to

389   31.0 (avg. 27.8). The ratio of *n*-C$_{29}$ to *n*-C$_{27}$ varies from 0.50 to 1.37 (avg. 0.80). The total abundance

390   of *n*-alkanes averages 72.7 µg/gTOC, with a range of 2.7 µg/gTOC to 316.6 µg/gTOC

391   (Supplementary table 1).

392   Pearson's correlation coefficients show the strongest correlations exist between CPI and *n*-

393   C$_{29}$/*n*-C$_{27}$ ($r = 0.809$, $p < 0.0000$), and ACL and *n*-C$_{29}$/*n*-C$_{27}$ ($r = 0.825$, $p < 0.0000$) (Fig. 12). Weak

394   correlations exist between the total abundance of *n*-alkanes and the other three variables considered;

395   CPI, ACL and *n*-C$_{29}$/*n*-C$_{27}$ ($r = 0.350$, $p = 0.0461$; $r = 0.396$, $p = 0.0224$; $r = 0.389$, $p = 0.0338$

396   respectively). Only one combination, CPI and ACL, does not indicate a statistically significant

397   correlation, as ACL becomes much more variable at low CPIs. Facies 11 has significantly lower CPI

398   and higher *n*-C$_{29}$/*n*-C$_{27}$ than facies 10 (Fig. 6). ACL is much more variable in facies 11, and on

399   average higher, while the total abundance of *n*-alkanes is on average lower than facies 10.

400   One sample from facies 11 was analysed for additional biomarkers (Supplementary table 2).

401   The sample contained a range of thermally mature C$_{27}$–C$_{35}$ hopanes. The dominant compounds were

402   17α,21β(H)-norhopane (C$_{29}$) and 17α,21β(H)-hopane (C30). This sample was characterised by low

403   ββ/(αβ+βα+ββ) ratios (0), high C22S/C22R+C22S ratios (0.57) and moderate Ts/Ts+Tm ratio (0.31).

404   Collectively, this indicates high thermal maturity.
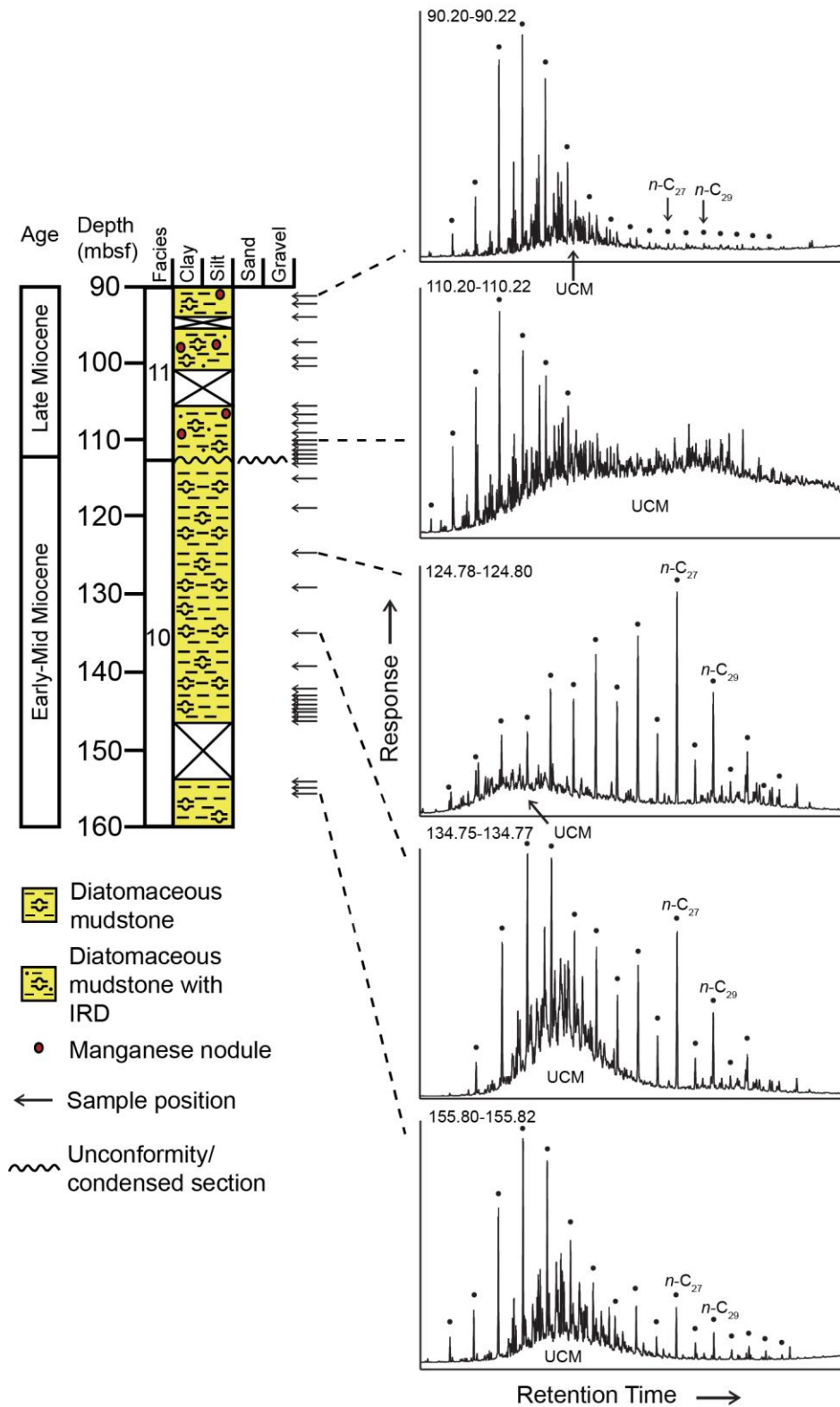
Fig. 11. Stratigraphic column from DSDP 274 with the stratigraphic positions of representative GC-FID-chromatograms of samples. Filled circles above peaks indicate n-alkanes, with the n-C_{27} and n-C_{29} labelled. Facies are described in table 1. UCM: unresolved complex mixture.

405

406

407

408

409
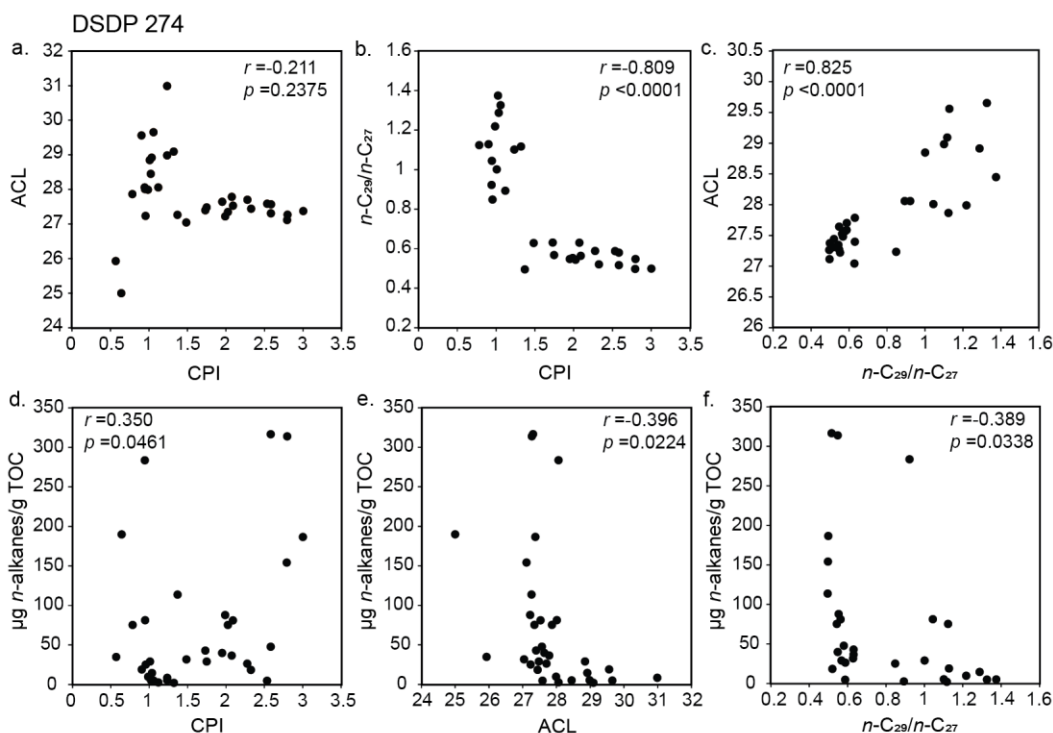
Fig. 12. Scatter plots of samples from DSDP 274; a) CPI and ACL; b) CPI and n-C_{29}/n-C_{27};
c) n-C_{29}/n-C_{27} and ACL; d) CPI and the total abundance of n-alkanes (μg n-alkanes/g TOC); e) ACL
and the total abundance of n-alkanes (μg n-alkanes/g TOC) and f) n-C_{29}/n-C_{27} and the total
abundance of n-alkanes (μg n-alkanes/g TOC).

4 Discussion

4.1 Potential sources of lipid biomarkers in Cenozoic Antarctic sediments

4.1.1 Contemporaneous organic matter

Plants and microorganisms living contemporaneously with the accumulation of sediment
would have been a major contributing source for n-alkanes and hopanes with ββ stereochemistry at
the sites studied. Macro- and microfossils from sediment cores, onland outcrops and glacial erratics
indicate that the Ross Sea region of Antarctica was vegetated until at least the Mid-Miocene Climate
Transition (MMCT) ~14 Ma (e.g. Kemp, 1975; Mildenhall, 1989; Askin, 2000; Askin and Raine,
2000; Lewis et al., 2008; Warny et al., 2009; Lewis and Ashworth, 2016). Paleocene and Early
Eocene sediment from cores offshore Wilkes Land indicate a highly diverse, near tropical flora
occupied coastal regions, with temperate rain forest inland and at higher elevations (Pross et al.,
2012). Following a prolonged period of global cooling, sediments from the Ross Sea region indicate
that by the Mid-Late Eocene, vegetation was largely represented by a less diverse, cool, temperate
flora dominated by *Nothofagus*-podocarpaceous conifer-proteaceae (Askin, 2000; Francis, 2000; Pole
et al., 2000).

22

429   The Oligocene and early Miocene was marked by declining vegetation diversity and the

430   development of a sparse, shrubby tundra, dominated by stunted *Nothofagus* (Kemp, 1975; Kemp and

431   Barrett, 1975; Askin and Raine, 2000; Prebble et al., 2006a). The Mid-Miocene Climate Optimum

432   (MMCO) (~17-15 Ma), saw an increase in the abundance of pollen transported offshore indicating a

433   proliferation of woody vegetation and a possible return to more tree-like forms (Warny et al., 2009;

434   Feakins et al., 2012). This short-lived warming was followed by the MMCT, a major cooling step in

435   the Cenozoic (Shackleton and Kennett, 1975; Flower and Kennett, 1994; Lewis et al. 2007). The

436   vegetation history of Antarctica following the MMCT has been debated, with different schools of

437   thought suggesting that demise of higher plants occurred either at the MMCT (Sugden et al., 1993;

438   Marchant et al., 1996; Lewis et al., 2008) or the Pliocene (Harwood et al. 1983; Webb et al. 1984;

439   Fielding et al., 2012). The Pliocene ages are controversial and rely on sparse diatoms present in tills of

440   the Meyer Desert Formation, preserved in the upper Beardmore Glacier (Barrett, 2013).

441   *4.1.2 Reworked lipid biomarkers from older sediments*

442   Lipid biomarkers could also be sourced from the erosion and redeposition of older sediments.

443   Two main sources are considered here; reworked Cenozoic *n*-alkanes, and reworked Permian-Jurassic

444   biomarkers sourced from the Beacon Super Group and Ferrar Group. The presence of Cretaceous

445   dinoflagellate cysts in samples of the McMurdo erratics suggests the possibility for a contribution

446   from rocks of this age now either eroded or buried, but as these occurrences are extremely rare this

447   potential contribution is considered very minor (Askin, 2000). Surface sediment from the Eastern

448   Ross Sea does contain a significant component of Late Cretaceous palynomorphs, but the location of

449   DSDP Site 270 in the central Ross Sea does not (Truswell and Drewry, 1984). Oligocene/Late

450   Miocene sediments in this core are also barren of pollen from this time period (Kemp, 1975; Duncan,

451   2017).

452   Microfossil work on Oligocene and Miocene sediments in continental margin drillcores

453   frequently indicate the presence of older Cenozoic microfossils, likely eroded from older sedimentary

454   basin infill. In particular, Eocene aged dinoflagellate cysts of the 'Transantarctic flora' are used to

455   infer reworking of Eocene material into younger sediments (e.g. Kemp, 1975; Askin and Raine, 2000;

456   Prebble et al., 2006a). Limited burial of Cenozoic sediments means that Paleogene forms reworked

457   into younger sediments are still light in colour and display similar autofluorescence (e.g. Askin and

458   Raine, 2000; Prebble et al., 2006a). Here, *n*-alkanes extracted from the fossiliferous McMurdo erratics

459   serve as an indication of typical Mid-Late Eocene distributions of these compounds (Section 4.2.1).

460   The Beacon Supergroup extends throughout the TAM and is a key source of sediment to the

461   sedimentary basins of the Ross Sea (e.g. Talarico et al., 2000; Smellie, 2001; Sandroni and Talarico,

462   2004; Sandroni and Talarico, 2011). Many of the fossil assemblages from the Beacon Supergroup

463   come from widespread Permian and Triassic sediments, and indicate a cool, humid Mid-Late Permian

464 climate with vegetation dominated by *Glossopteris* and *Gangamopteris* (Cúneo et al., 1993; Francis et

465 al., 1994; Collinson, 1997). By the Mid-Triassic, a more diverse flora dominated by *Dicroidium*

466 indicates a shift to warmer 'greenhouse' conditions (Collinson, 1997; Cúneo et al., 2003). The Beacon

467 Supergroup outcropping in the TAM has undergone widespread intrusion and thermal alteration, with

468 altered palynomorphs in continental margin cores likely reflecting a TAM source, whilst less altered

469 specimens must have been transported from less extensively intruded sediments cratonwards of the

470 TAM (Askin, 1998; Askin and Raine, 2000). Fossiliferous sedimentary interbeds of the Jurassic

471 Ferrar group are also known to contribute reworked palynomorphs to offshore sediments, albeit with

472 much rarer occurrences than those sourced from the Beacon Supergroup (Askin and Raine, 2000). *n*-

473 Alkanes have previously been analysed from Beacon sediments, silicified wood and coal at the Allan

474 Hills and Ferrar Group sediments from Carapace Nunatak in Southern Victoria Land (Matsumoto et

475 al., 1986). *n*-Alkanes ranging from n-C_{12} to n-C_{30} displayed a CPI varying from 0.91-1.4. Short chain

476 *n*-alkanes ($< n$-C_{20}) were typically more abundant than long chain lengths (Matsumoto et al., 1986). A

477 chromatogram from Matsumoto et al. (1986) indicates that UCMs are also present in these samples,

478 centred at n-C_{18} and n-C_{19}. Hopanes in these Beacon sediments were typically dominated by αβ and

479 βα configurations indicating maturation of the sediments and alteration of hopanes from their

480 biologically synthesized precursors (Matsumoto et al., 1987). Variable thermal maturation of the

481 Beacon sediments in this region is suggested by two samples containing small quantities of ββ

482 hopanes (Matsumoto et al., 1987)

483   Distributions of *n*-alkanes, kerogen and palynomorphs in surface and Quaternary sediments

484 from the Ross Sea, and soils from the Dry Valleys, suggest the potential for recycling of *n*-alkanes

485 from both Cenozoic and pre-Cenozoic sources is occurring via modern depositional processes. In the

486 Ross Sea, *n*-Alkanes appear in low abundances with short chained *n*-alkanes attributed to a mixture of

487 primary and recycled material derived from marine organisms, while long chained *n*-alkanes are

488 suggested to be higher plant material either from long-range aeolian transport or reworked from pre-

489 Quaternary sediments (Kvenvolden et al., 1987; Venkatesan, 1988). A recycled source for *n*-alkanes

490 is supported by the presence of hopanes of variable maturities (ββ, βα and αβ), and kerogen and

491 pollen extensively reworked from Paleogene or pre Cenozoic sediment (Sackett et al., 1974; Truswell

492 and Drewry, 1984, Kvenvolden et al., 1987). The most abundant *n*-alkanes in soils from the Dry

493 Valleys are usually n-C_{23}, n-C_{25}, or n-C_{27} (Matsumoto et al., 1990a; Matsumoto et al., 2010; Hart et

494 al., 2011). *n*-Alkanes are attributed to a mixed source input, predominantly derived from endolithic

495 microorganisms and glacially eroded ancient plant and microorganism debris, sourced from earlier

496 Cenozoic sediments and the Beacon Sandstone (Matsumoto et al., 1990a; Matsumoto et al., 2010).

497 This is supported by the presence of mature (βα and αβ) isomers of hopanes, likely sourced from

498 Beacon sediments (Matsumoto et al., 1990b) Aeolian transport as a main source for the *n*-alkanes in

499 these samples is considered unlikely, as aerosol samples near Antarctica record *n*-alkane distributions

500   with high ACLs and a dominant n-C_{31}, potentially as a result of large scale meridional air mass

501   circulation transporting n-alkanes from the tropics to high latitudes (Bendle et al., 2007).

4.1.3 In situ degradation of n-alkanes

503   In Antarctica and the Sub-Antarctic, hydrocarbon contamination experiments indicate that

504   hydrocarbon degrading microbes are present in soils (Aislabie et al., 1998; Bej et al., 2000; Coulon et

505   al., 2005). Longer chain length n-alkanes were found to be more resistant to microbial degradation,

506   and rates of degradation increase with increasing temperature (Coulon et al., 2005). n-Alkane

507   distributions in the studied samples are not considered the result of *in situ* thermal maturation, or

508   migration of hydrocarbons into the sediments. The sediment sampled in this study comes from near

509   surface sediment in the case of Mt Boreas, or drill cores where the deepest samples come from 385

510   mbsf in DSDP 270. None of the studied cores contained hydrocarbon residues, and heat flow

511   measurements from CRP-2/2A and other cores in the region (CRP 3, ANDRILL 1B, ANDRILL 2A)

512   range from 24-76.7 °C/km (Bücker et al., 2000; Bücker et al., 2001; Morin et al., 2010; Schröder et

513   al., 2011). Basin modelling from the central and western Ross Sea shows that while the generation of

514   hydrocarbons is possible in the deeply buried sediments of the basins, expulsion and migration of

515   hydrocarbons from potential source rocks is very unlikely (Strogen and Bland, 2011).

4.2 n-Alkane distributions across sample sites

4.2.1 McMurdo erratics

518   The McMurdo erratics provide examples of mid-late Eocene n-alkane distributions, when

519   Antarctic vegetation was more diverse than in the Oligocene and Miocene, and the climate was

520   warmer and wetter (Askin, 2000; Francis, 2000; Pole et al., 2000). All of the samples except for

521   MTD95 contain a terrestrial palynomorph assemblage, with E215 and E219 also including leaves and

522   in E219, wood macrofossils (Harwood and Levy, 2000). However, these erratics do also contain a

523   minor component of reworked material sourced from the Beacon Supergroup (Askin, 2000). Despite

524   this, the occurrence of macro-fossils and dominantly Eocene-aged assemblages of palynomorphs

525   suggest that the n-alkanes in these samples are principally from contemporaneously-sourced organic

526   matter. The key difference in the n-alkane distributions of the McMurdo erratics compared to

527   Oligocene and Miocene samples from the other studied sites is the prominence of the n-C_{29} as

528   opposed to the n-C_{27} (Supplementary table 1, Fig.3). We suggest the shift from a dominant n-C_{29} to n-

529   C_{27} in the Ross Sea region is due to a combination of climate cooling as the Antarctic ice sheets

530   developed, and a shift in plant community to a flora dominated by a low diversity tundra of

531   *Nothofagus, podocarpidites* and bryophytes (Askin, 2000; Askin and Raine, 2000; Prebble et al.,

532   2006a; Lewis et al., 2008).

25

4.2.2 Mt Boreas

534   The presence of macro and microfossils of bryophytes at Mt Boreas is represented by the

535   prominence of n-C$_{23}$ and n-C$_{25}$ in the n-alkane distributions from this site (Fig. 4) (Lewis et al., 2008).

536   The n-C$_{27}$ homolog is also particularly abundant and is likely sourced from shrubs and trees such as

537   *Nothofagidites lachlaniae* in the lake catchment (Lewis et al., 2008). A correlation between increasing

538   n-C$_{29}$ and decreasing CPI could be the result of either: 1) microbial degradation lowering CPI and

539   preferentially degrading the shorter chain n-C$_{27}$; or 2) incorporation of recycled material, likely from

540   weathered, thermally-degraded Beacon Supergroup, and older Cenozoic sediments in the catchment.

541   This is supported by the presence of thermally matured hopanes in sample ALS-05 21O, which is

542   from the base of the lacustrine section, just above a glacial till containing clasts of Beacon Supergroup

543   (Lewis et al., 2008). Other samples in which hopanes were investigated were dominated by ββ

544   hopanes, supporting an interpretation that much of the biomarkers in the rest of the lacustrine

545   sediments are contemporaneously sourced. Lacustrine depositional environments (Facies 1) have

546   higher average CPIs and lower average n-C$_{29}$/n-C$_{27}$ values than fluvial samples (Facies 2) (Fig. 6).

547   Fluvial environments can be erosive settings as coarser sediments require greater water velocity for

548   suspension and movement (Miller et al., 1977), suggesting a fluvially influenced environment is more

549   likely to rework n-alkanes. In the lacustrine setting, high CPI, low ACL and n-C$_{29}$/n-C$_{27}$ in particular

550   occur directly below, and almost directly above the moss peat (Fig. 4). n-alkane distributions are

551   likely sampling the aquatic plants and mosses deposited during a shallow water phase of the lake.

552   Samples from beds representing a deeper water phase of the lake (Lewis et al., 2008) are marked by a

553   similar average CPI and n-C$_{29}$/n-C$_{27}$ as the laminated silts, but a higher ACL, reflecting an increased

554   input of emergent and terrestrial plant matter from the surrounding catchment.

555   *4.2.3 CRP 2/2A*

556   In CRP 2/2A, n-alkane distributions typically show the n-C$_{27}$ as the dominant homolog,

557   although n-C$_{23}$, n-C$_{25}$ and n-C$_{29}$ were also commonly abundant. The prominence of these n-alkane

558   homologs is in line with palynomorph evidence which suggests input from trees, shrubs and

559   bryophytes (Prebble et al., 2006a). Fluctuating abundances of reworked palynomorphs (thermally

560   altered, poorly preserved or of a known older range) often coincide with larger abundances of Eocene

561   Transantarctic flora dinoflagellates (Prebble et al., 2006a). This indicates reworked samples were

562   sourced from both Permian/Triassic Beacon sediments and earlier Cenozoic sediments. The

563   correlations between low CPI, and high ACL and n-C$_{29}$/n-C$_{27}$ (Fig. 8) can be explained by a mixed

564   source input of n-alkanes, from contemporaneous material, early Cenozoic sediments, and both

565   altered and unaltered areas of the Beacon Supergroup. This is supported by the presence of both

566   biologically synthesized and thermally matured hopane configurations. While a contribution from

567   more recent recycled material (i.e Early Oligocene n-alkanes) cannot be ruled out, Prebble et al.

568   (2006b) found little evidence for reworking between Early and Late Oligocene sequences. UCMs in

569   these samples typically underlie the lower chain lengths, and may be the result of post-depositional

570   microbial alteration, or could be inherited from the Beacon Supergroup (Matsumoto et al., 1986).

571   Facies groupings reflect depositional environments which are predominantly influenced by the

572   proximity of glaciers near the site. More ice-distal, marine facies (7 and 8) have on average high CPIs,

573   low ACL and low n-C$_{29}$/n-C$_{27}$ (Fig. 6), while samples from ice-proximal or subglacial settings tend to

574   show the opposite trends. This suggests that low-energy, more ice-distal marine environments are

575   more likely to contain well-preserved n-alkane distributions reflecting contemporaneously sourced n-

576   alkanes, whilst more ice-proximal and subglacial environments have a higher likelihood of containing

577   reworked n-alkanes.

578   *4.2.4 DSDP 270*

579   n-Alkane distributions from DSDP 270 are typically bi-modal suggesting two primary sources

580   for n-alkanes in this drill core (Fig. 9). Algae and bacteria the likely source for the shorter chain

581   lengths, with terrestrial higher plants contributing to longer chain lengths (section 2.5). The presence

582   of a contemporaneous pollen assemblage with almost no reworked contribution indicates the long

583   chained n-alkanes predominantly reflect contemporary onshore vegetation. This is shown in the CPI

584   values that vary less than the other sites sampled and all sit above 2.4 (Fig. 6), and the predominance

585   of hopanes in ββ configurations. Facies representing more ice-proximal settings (facies 3 and 4) show

586   the lowest average CPIs suggesting that these settings are likely to contain more degraded n-alkane

587   distributions, whether as the result of post-depositional processes or some sediment recycling due to

588   glacial erosion and redeposition (Fig. 6).

589   *4.2.5 DSDP 274*

590   n-Alkane distributions in DSDP 274 are separated into two distinct groups, above and below

591   an unconformity/condensed section at 113.6 mbsf (Figs. 6 and 11). Samples taken from below 113.6

592   mbsf show bi-modal distributions in chromatograms suggesting a mixed contribution from both algae

593   and bacteria, and terrestrial plants. Other than the uppermost 2 samples from this section of the core,

594   all samples are considered to be part of facies 10, which was deposited with a high terrigenous and

595   biogenic sedimentation rate, under a regime of weak bottom currents (Fig. 2) (Frakes, 1975;

596   Whittaker and Müller, 2006). Reworked palynomorphs are present in this section (Kemp, 1975),

597   which, coupled with variable CPI and UCMs suggest that some contribution of reworked n-alkanes is

598   likely. However, the generally high CPI, dominance of the n-C$_{27}$ and lack of variation in ACL and n-

599   C$_{29}$/n-C$_{27}$ suggests that much of the n-alkanes present reflect comparatively more contemporaneous

600   input than the overlying interval, or at least material recycled from the Oligocene or younger.

Above the unconformity or condensed section at 113.6 mbsf, the sedimentation rate slows and manganese nodules provide evidence for winnowing by a strong bottom current regime. This interval is also associated with an increase in coarse sediment which could result from ice rafting (Frakes, 1975; Whittaker and Müller, 2006) or winnowing of the fine fraction due to intensification of bottom currents. These sediments date to the Late Miocene, and Antarctic glacial expansion at this time could explain the increase in ice rafting or bottom water current intensity (McKay et al., 2009; Herbert et al., 2016). Sediments from this part of the core are also include and post-date the MMCT when it has been debated that higher plants became extinct on Antarctica (Sugden et al., 1993; Marchant et al., 1996; Lewis et al., 2008). This indicates that n-alkanes from this section of the core may predominantly be derived from older sediments, an interpretation supported by a hopane distribution dominated by thermally matured configurations. Low CPIs, high n-C_{29}/n-C_{27}, often large and dominant UCMs and low sedimentation rates suggest that n-alkanes in these samples have also been extensively degraded, likely by microbial activity as sediments are winnowed and reworked in the surface layers of the seabed.

5. Synthesis

n-Alkane distributions in Eocene to Miocene sediments from the Ross Sea region vary with age and sample site. Between the Eocene and Oligocene, the dominant chain length recorded in sediments changes from n-C_{29} to n-C_{27}, concomitant with a significant climate cooling and a shift in plant community (section 4.2.1). The dominance of the n-C_{27} in sediments sourced from wide catchments incorporating a cool, low diversity vegetation dominated by *Nothofagus* is in contrast to lower latitudes where n-C_{29} and n-C_{31} are often more abundant (e.g. Poynter et al., 1989; Kawamura et al., 2003; Sachse et al., 2006; Bendle et al., 2007). At least one modern species of *Nothofagus* (*N. menziesii*) from New Zealand has been shown to produce n-C_{27} as its dominant n-alkane (Burrington, 2015), while other species in New Zealand and South America are typically dominated by n-C_{29} and n-C_{31} (Schellekens et al., 2009; Schellekens et al., 2011; Burrington, 2015). The high abundance of n-C_{27} in samples from Mt Boreas also containing abundant pollen from *N. lachlaniae* suggest that this species was likely producing large proportions of this n-alkane. The prominence of the n-C_{27} across the Oligocene and Miocene sites of this study likely reflects both a climate adaption by plants growing in the Antarctic tundra to cold temperatures, and the abundance of *Nothofagus* in the catchments.

While the Oligocene and Miocene vegetation of Antarctica was a main source of n-alkanes to the sample sites, reworked n-alkanes and hopanes from early and pre-Cenozoic sediments were also evident. In particular, variables that often characterised samples with more reworked material were low CPI values, but higher ACLs and n-C_{29}/n-C_{27} ratios. In a sample containing material solely from reworked thermally altered sections of the Beacon Supergroup, a low CPI, ACL and n-C_{29}/n-C_{27}

636 would be expected (Matsumoto et al., 1986). The association of low CPIs with high ACL and n-C_{29}/n-

637 C_{27} therefore suggests that reworked samples likely contain a mixture of n-alkanes derived from

638 thermally matured Beacon sediments, coupled with material from early Cenozoic and less altered pre-

639 Cenozoic sediments containing a higher abundance of longer chained n-alkanes such as n-C_{29} and n-

640 C_{31}. In some instances, this distribution could also result from microbial degradation, which could

641 lower CPI, whilst also preferentially scavenging shorter chain lengths.

642   Sediments deposited by glacio-fluvial, ice-proximal glaciomarine and subglacial processes

643 are more likely to contain reworked n-alkane distributions than those from lacustrine or ice-distal

644 marine environments, although careful site specific consideration of sediment provenance must be

645 undertaken, regardless of relative proximity to glaciers or rivers. Prior to the MMCT, glaciers

646 throughout the TAM, and likely the exposed areas of the Ross Sea, were warm-based (Marchant and

647 Denton, 1996; Lewis et al., 2007). This regime would have favoured high rates of glacial erosion of

648 underlying strata, resulting in rapid remobilisation, deposition and burial of sediment in glacial

649 proximal regions (Sugden and Denton, 2004; Powell et al. 2000). These processes likely led to the

650 deposition of greater proportions of reworked n-alkanes in ice-proximal environments. Although ice-

651 distal settings also record glaciomarine processes and may be subject to reworking, they are likely a

652 more integrated record of aeolian and glacio-fluvial sediment transport offshore. However, as

653 Antarctica became progressively more arid during the Late Miocene and Pliocene, it is feasible that

654 offshore transport of contemporaneous n-alkanes via glacio-fluvial action reduced, and thus the

655 relative input of reworked n-alkanes became more prominent (e.g. at DSDP 274).

656   The varying contribution of contemporaneous and reworked biomarkers across sediments

657 sourced from different depositional environments, catchments and ages emphasizes how caution must

658 be exercised when applying biomarker-based paleoclimate proxies in glacially-influenced settings

659 (e.g. n-alkane $\delta^{13}C$ and δ^2H). In particular, several aspects should be considered when determining if

660 an n-alkane distribution is a contemporaneously-sourced organic matter signature. These include the

661 values and variation of factors such as CPI and ACL, maturation indices of other biomarkers such as

662 hopanes, whether the catchment and depositional setting of a site is more likely to accumulate and

663 preserve a contemporary distribution, and assemblages of other fossil material such as palynomorphs.

664 When constructing timeseries of biomarker assemblages, it is also important to consider other aspects

665 of the depositional environment in the Ross Sea. The coastal setting of the Ross Sea could be

666 influenced by pulses of reworked material, given the potential for point source glacial meltwater

667 discharge, and large-scale meltwater discharge events (i.e. Powell and Domack, 2002; Lewis et al.,

668 2006), which may focus erosion to a certain lithological source. Input of reworked material via

669 episodic, erosive hydrological events in Paleocene-Eocene Thermal Maximum sediments from

670 Tanzania has been invoked to explain the highly variable n-alkane $\delta^{13}C$ values in these sediments

671 (Carmichael et al., 2017). Glacially-influenced environments have a high potential to erode and

29

672 almost instantaneously redeposit older biomarkers and pollen offshore in concentrated numbers, and

673 indeed biomarker distributions could be used as a potential tool to identify such reworking events.

6 Conclusions

675 n-Alkane and hopanoid distributions have been characterised in Eocene to Miocene sediments

676 from a range of depositional environments in the Ross Sea region of Antarctica. Between the Late

677 Eocene and the Oligocene, a shift in n-alkane dominant chain length is observed from n-C_{29} to n-C_{27}.

678 This is inferred to be a result of both a shift in plant community, as well as a response to significant

679 climate cooling. Biomarker distributions in Oligocene and Miocene samples varyingly display a

680 contribution from both contemporaneous and reworked sources. n-Alkane distributions typical of a

681 reworked sample were a low CPI, and high ACL and n-C_{29}/n-C_{27} values. Reworked samples likely

682 reflect a mixed contribution from thermally altered and less thermally altered regions of the Mesozoic

683 Beacon Super Group, coupled with material sourced from earlier Cenozoic sediments. Microbial

684 degradation during transport and post-deposition may also contribute to these distributions. Samples

685 dominated by contemporaneously-sourced organic matter display a higher CPI, and lower ACL and n-

686 C_{29}/n-C_{27} values. These n-alkanes were sourced from the sparse, cold tundra which existed during this

687 time. Fluvial environments onshore, and subglacial and ice-proximal environments offshore were

688 more likely to contain reworked n-alkanes. Lacustrine environments onshore, and ice-distal

689 environments offshore, were more likely to contain contemporary n-alkanes. These findings indicate

690 the possibility of reworking should be taken into account when biomarkers are used for paleoclimate

691 studies in ice-marginal environments.

Data Availability

702 Data associated with this study can be found in the supplementary tables.

References

704 Aislabie, J., McLeod, M., Fraser, R., 1998. Potential for biodegradation of hydrocarbons in soil from
705   the Ross Dependency, Antarctica. Applied Microbiology and Biotechnology 49, 210-214.

706 Allibone, A.H., Cox, S.C., Graham, I.J., Smillie, R.W., Johnstone, R.D., Ellery, S.G., Palmer, K.,
707   1993. Granitoids of the Dry Valleys area, southern Victoria Land, Antarctica: plutons, field
708   relationships, and isotopic dating. New Zealand journal of geology and geophysics 36, 281-297.

709 Allibone, A.H., Cox, S.C., Smillie, R.W., 1993. Granitoids of the Dry Valleys area, southern Victoria
710   Land: geochemistry and evolution along the early Paleozoic Antarctic Craton margin. New
711   Zealand journal of geology and geophysics 36, 299-316.

712 Askin, R.A., 1998. Palynological investigations of Mount Feather Sirius Group samples: recycled
713   Triassic assemblages, In: Wilson, G.S., Barron, J. (Eds.), Mount Feather Sirius Group Core
714   Workshop and Collaborative Sample Analysis. Byrd Polar Research Center Report No. 14.
715   Byrd Polar Research Center, The Ohio State University, Columbus, Ohio, pp. 59-65.

716 Askin, R.A., 2000. Spores and pollen from the McMurdo Sound erratics, Antarctica. In: Stilwel, J.D.,
717   Feldman, R.M. (Eds.), Paleobiology and Paleoenvironments of Eocene Rocks: McMurdo
718   Sound, East Antarctica. American Geophysical Union, Washington, D.C., pp. 161-181.

719 Askin, R.A., Raine, J.I., 2000. Oligocene and Early Miocene terrestrial palynology of the Cape
720   Roberts Drillhole CRP-2/2A, Victoria Land Basin, Antarctica. Terra Antarctica 7, 493-501.

721 Barrett, P.J., 1981. History of the Ross Sea region during the deposition of the Beacon Supergroup
722   400-180 million years ago. Journal of the Royal Society of New Zealand 11, 447-458.

723 Barrett, P.J., Elliot, D.H., Lindsay, J.F., 1986. The Beacon Supergroup (Devonian- Triassic) and
724   Ferrar Group (Jurrasic) in the Beardmore Glacier Area, Antarctica. In: Turner, M.D.,
725   Splettstoesser J.E. (Eds.), Geology of the central Transantarctic Mountains. American
726   Geophysical Union, Washington, D.C., pp. 339-428.

727 Barrett, P.J. (Ed.). 1989. Antarctic Cenozoic history from the CIROS-1 drillhole, McMurdo Sound.
728   DSIR Publishing, Wellington, New Zealand.

729 Barrett, P.J., 2013. Resolving views on Antarctic Neogene glacial history–the Sirius debate. Earth and
730   Environmental Science Transactions of the Royal Society of Edinburgh 104, 31-53.

731 Bej, A.K., Saul, D., Aislabie, J., 2000. Cold-tolerant alkane-degrading Rhodococcus species from
732   Antarctica. Polar Biology 23, 100-105.

733 Bendle, J., Kawamura, K., Yamazaki, K., Niwai, T., 2007. Latitudinal distribution of terrestrial lipid
734   biomarkers and n-alkane compound-specific stable carbon isotope ratios in the atmosphere over
735   the western Pacific and Southern Ocean. Geochimica et Cosmochimica Acta 71(24), 5934-
736   5955.

737 Bijl, P.K., Bendle, J.A., Bohaty, S.M., Pross, J., Schouten, S., Tauxe, L. Stickley, C.E., McKay, R.M.,
738   Röhl, U., Olney, M., Sluijs, A., Escutia, C., Brinkhuis, H., Expedition 318 Scientists, 2013.

739   Eocene cooling linked to early flow across the Tasmanian Gateway. Proceedings of the

740   National Academy of Sciences 110, 9645-9650.

741 Bray, E.E., Evans, E.D., 1961. Distribution of n-paraffins as a clue to recognition of source

742   beds. Geochimica et Cosmochimica Acta 22, 2-15.

743 Bücker, C.J., Wonik, T., Jarrard, R., 2000. The temperature and salinity profile in CRP-2/2A, Victoria

744   Land Basin, Antarctica. Terra Antarctica 7, 255-259.

745 Bücker, C., Jarrard, R.D., Wonik, T., 2001. Downhole temperature, radiogenic heat production, and

746   heat flow from the CRP-3 drillhole, Victoria Land Basin, Antarctica. Terra Antarctica 8, 151-

747   160.

748 Burrington, P., 2015. How to be a Prehistoric Weatherman: Using n-alkanes as a Proxy for Holocene

749   Climate and Hydrology, Southwest South Island, New Zealand (Unpublished Masters Thesis).

750   University of Otago, New Zealand.

751 Bush, R.T., McInerney, F.A., 2013. Leaf wax n-alkane distributions in and across modern plants:

752   implications for paleoecology and chemotaxonomy. Geochimica et Cosmochimica Acta 117,

753   161-179.

754 Bush, R.T., McInerney, F.A., 2015. Influence of temperature and C_4 abundance on n-alkane chain

755   length distributions across the central USA. Organic Geochemistry 79, 65-73.

756 Calvo, E., Pelejero, C., Logan, G.A., De Deckker, P., 2004. Dust-induced changes in phytoplankton

757   composition in the Tasman Sea during the last four glacial cycles. Paleoceanography 19.

758 Cape Roberts Science Team, 1999. Studies from the Cape Roberts Project, Ross Sea Antarctica,

759   Initial report on CRP-2/2A. Terra Antarctica 6(1), 1-173.

760 Carmichael, M. J., Inglis, G. N., Badger, M. P., Naafs, B. D. A., Behrooz, L., Remmelzwaal, S.,

761   Monteiro, F. M., Rohrssen, M., Farnsworth, A., Buss, H. L., Dickson, A. J., Valdes, P. J., Lunt,

762   D. J., Pancost, R. D., 2017. Hydrological and associated biogeochemical consequences of rapid

763   global warming during the Paleocene-Eocene Thermal Maximum. Global and Planetary

764   Change 157, 114-138.

765 Clark Jr, R.C., Blumer, M., 1967. Distribution of n-paraffins in marine organisms and

766   sediment. Limnology and Oceanography 12, 79-87.

767 Collinson, J.W., 1997. Paleoclimate of Permo-Triassic Antarctica. International Symposium on

768   Antarctic Earth Sciences 7, 1029-1034.

769 Cooper, A.K., Davey, F.J., Behrendt, J.C., 1987. Seismic stratigraphy and structure of the Victoria

770   Land basin, western Ross Sea, Antarctica. In: Cooper, A.K., Davey, F.J. (Eds.), The Antarctic

771   Continental Margin: Geology and Geophysics of the Western Ross Sea. Circumpacific Council

772   for Energy and Mineral Resources, Houston, T.X., pp. 27-65.

773 Coulon, F., Pelletier, E., Gourhant, L., Delille, D., 2005. Effects of nutrient and temperature on

774   degradation of petroleum hydrocarbons in contaminated sub-Antarctic soil. Chemosphere 58,

775   1439-1448.

776   Cranwell, P.A., Eglinton, G., Robinson, N., 1987. Lipids of aquatic organisms as potential
777   contributors to lacustrine sediments—II. Organic Geochemistry 11, 513-527.

778   Cúneo, N.R., Isbell, J., Taylor, E.L., Taylor, T.N., 1993. The Glossopteris flora from Antarctica:
779   taphonomy and paleoecology. Comptes Rendus XII ICC-P 2, 13-40.

780   Cúneo, N.R., Taylor, E.L., Taylor, T.N., Krings, M., 2003. In situ fossil forest from the upper
781   Fremouw Formation (Triassic) of Antarctica: paleoenvironmental setting and paleoclimate
782   analysis. Palaeogeography, Palaeoclimatology, Palaeoecology 197, 239-261.

783   Decesari, R.C., Sorlien, C.C., Luyendyk, B.P., Wilson, D.S., Bartek, L.R., Diebold, J., Hopkins, S.E.,
784   2007. Regional seismic stratigraphic correlations of the Ross Sea: implications for the tectonic
785   history of the West Antarctic Rift System. In: Cooper, A.K., Raymond, C.R., 10th ISAES
786   Editorial Team (Eds.), Antarctica: A Keystone in a Changing World- Online Proceedings of the
787   10th ISAES, 2007-1047, USGS Open-File Report, Short Research Paper 052, 4p.

788   De Santis, L., Anderson, J.B., Brancolini, G., Zayatz, I., 1995. Seismic record of late Oligocene
789   through Miocene glaciation on the central and eastern continental shelf of the Ross Sea. In:
790   Cooper, A.K., Barker, P.F., Brancolini, G. (Eds.), Geology and Seismic Stratigraphy of the
791   Antarctic Margin. American Geophysical Union, Washington, D.C., pp. 235-260.

792   Dodd, R.S., Rafii, Z.A., Power, A.B., 1998. Ecotypic adaptation in Austrocedrus chilensis in cuticular
793   hydrocarbon composition. New Phytologist 138, 699-708.

794   Dodd, R.S., Afzal-Rafii, Z., 2000. Habitat-related adaptive properties of plant cuticular
795   lipids. Evolution 54, 1438-1444.

796   Duncan, B.J., 2017. Cenozoic Antarctic climate evolution based on molecular and isotopic biomarker
797   reconstructions from geological archives in the Ross Sea region (Unpublished PhD Thesis).
798   Victoria University of Wellington, New Zealand.

799   Eglinton, G., Hamilton, R.J., 1963. The distribution of alkanes. Chemical plant taxonomy 187, 217.

800   Farrimond, P., Taylor, A., TelnÆs, N., 1998. Biomarker maturity parameters: the role of generation
801   and thermal degradation. Organic Geochemistry 29, 1181-1197.

802   Feakins, S.J., Warny, S., Lee, J.E., 2012. Hydrologic cycling over Antarctica during the middle
803   Miocene warming. Nature Geoscience 5, 557-560.

804   Feakins, S.J., Warny, S., DeConto, R.M., 2014. Snapshot of cooling and drying before onset of
805   Antarctic Glaciation. Earth and Planetary Science Letters 404, 154-166.

806   Feakins, S.J., Peters, T., Wu, M.S., Shenkin, A., Salinas, N., Girardin, C.A., Bentley, L.P., Blonder,
807   B., Enquist, B.J., Martin, R.E., Asner, G.P., Asner, G.P., 2016. Production of leaf wax n-
808   alkanes across a tropical forest elevation transect. Organic Geochemistry 100, 89-100.

809   Ficken, K.J., Li, B., Swain, D.L., Eglinton, G., 2000. An n-alkane proxy for the sedimentary input of
810   submerged/floating freshwater aquatic macrophytes. Organic Geochemistry 31, 745-749.

811   Fielding, C.R., Naish, T.R., Woolfe, K., Lavelle, M., 2000. Facies analysis and sequence stratigraphy
812   of CRP-2/2A, Victoria Land Basin, Antarctica. Terra Antarctica 7, 323-338.

813   Fielding, C.R., Henrys, S.A., Wilson, T.J., 2006. Rift history of the western Victoria Land Basin: a

814   new perspective based on integration of cores with seismic reflection data. In D.K. Fütterer, D.

815   Damaske, G. Kleinschmidt, H. Miller & F. Tessensohn (Eds.), Antarctica (pp. 309-318). Berlin

816   Heidelberg: Springer.

817   Fielding, C.R., Harwood, D.M., Winter, D.M., Francis, J.E., 2012. Neogene stratigraphy of Taylor

818   Valley, Transantarctic Mountains, Antarctica: evidence for climate dynamism and a vegetated

819   early Pliocene coastline of McMurdo Sound. Global and Planetary Change 96-97, 97-104.

820   Fitzgerald, P.G., 1994. Thermochronologic constraints on post-Paleozoic tectonic evolution of the

821   central Transantarctic Mountains, Antarctica. Tectonics 13, 818-836.

822   Flower, B.P., Kennett, J.P., 1994. The middle Miocene climatic transition: East Antarctic ice sheet

823   development, deep ocean circulation and global carbon cycling. Palaeogeography,

824   palaeoclimatology, palaeoecology 108, 537-555.

825   Frakes, L.A., 1975. Paleoclimatic significance of some sedimentary components at Site 274. Initial

826   Reports of the Deep Sea Drilling Project 28, 785-787.

827   Francis, J.E., Woolfe, K.J., Arnott, M.J., Barrett, P.J., 1994. Permian climates of the southern margins

828   of Pangea: evidence from fossil wood in Antarctica. Pangea: Global Environments and

829   Resources- Memoir 17, 275-282.

830   Francis, J.E., Hill, R.S., 1996. Fossil plants from the Pliocene Sirius Group, Transantarctic Mountains:

831   Evidence for climate from growth rings and fossil leaves. Palaios 11, 389-396.

832   Francis, J.E., 2000. Fossil Wood from Eocene High Latitude Forests: Mcmurdo Sound, Antarctica. In:

833   Stilwel, J.D., Feldman, R.M. (Eds.), Paleobiology and Paleoenvironments of Eocene Rocks:

834   McMurdo Sound, East Antarctica. American Geophysical Union, Washington, D.C., pp. 253-

835   260.

836   Gagosian, R.B., Peltzer, E.T., 1986. The importance of atmospheric input of terrestrial organic

837   material to deep sea sediments. Organic Geochemistry 10, 661-669.

838   Goodge, J.W., Myrow, P., Williams, I.S., Bowring, S.A., 2002. Age and provenance of the

839   Beardmore Group, Antarctica: constraints on Rodinia supercontinent breakup. The Journal of

840   geology 110, 393-406.

841   Gough, M.A., Rowland, S.J., 1990. Characterization of unresolved complex mixtures of hydrocarbons

842   in petroleum. Nature 344, 648-650.

843   Gough, M.A., Rhead, M.M., Rowland, S.J., 1992. Biodegradation studies of unresolved complex

844   mixtures of hydrocarbons: model UCM hydrocarbons and the aliphatic UCM. Organic

845   Geochemistry 18, 17-22.

846   Grimalt, J., Albaigés, J., Al-Saad, H.T., Douabul, A.A.Z., 1985. n-Alkane distributions in surface

847   sediments from the Arabian Gulf. Naturwissenschaften 72, 35-37.

848 Grimalt, J., Albaigés, J., 1987. Sources and occurrence of C_{12}-C_{22} n-alkane distributions with even
849   carbon-number preference in sedimentary environments. Geochimica et Cosmochimica Acta
850   51, 1379-1384.

851 Hambrey, M.J., Barrett, P.J. 1993. Cenozoic sedimentary and climatic record, Ross Sea region,
852   Antarctica. In: Kennett, J.P., Warnke, D.A. (Eds.) The Antarctic Paleoenvironment: A
853   Perspective on Global Change: Part Two, American Geophysical Union, Washington, D.C., pp.
854   91-124.

855 Han, J., Calvin, M., 1969. Hydrocarbon distribution of algae and bacteria, and microbiological
856   activity in sediments. Proceedings of the National Academy of Sciences 64, 436-443.

857 Hart, K.M., Szpak, M.T., Mahaney, W.C., Dohm, J.M., Jordan, S.F., Frazer, A.R., Allen, C.C.R.,
858   Kelleher, B.P., 2011. A bacterial enrichment study and overview of the extractable lipids from
859   paleosols in the Dry Valleys, Antarctica: implications for future Mars
860   reconnaissance. Astrobiology 11, 303-321.

861 Harwood, D.M., 1983. Diatoms from the Sirius Formation, Transantarctic Mountains. Antarctic
862   Journal of the United States 18, 98-100.

863 Harwood, D.M., Levy, R.H., 2000. The McMurdo Erratics: introduction and overview. In: Stilwel,
864   J.D., Feldman, R.M. (Eds.), Paleobiology and Paleoenvironments of Eocene Rocks: McMurdo
865   Sound, East Antarctica, American Geophysical Union, Washington, D.C., pp. 1-18.

866 Herbert, T.D., Lawrence, K.T., Tzanova, A., Peterson, L.C., Caballero-Gill, R., Kelly, C.S., 2016.
867   Late Miocene global cooling and the rise of modern ecosystems. Nature Geoscience 9, 843-
868   847.

869 Inglis, G. N., Naafs, B. D. A., Zheng, Y., McClymont, E. L., Evershed, R. P., Pancost, R. D., 2018.
870   Distributions of geohopanoids in peat: Implications for the use of hopanoid-based proxies in
871   natural archives. Geochimica et Cosmochimica Acta 224, 249-261.

872 Kawamura, K., Ishimura, Y., Yamazaki, K., 2003. Four years' observations of terrestrial lipid class
873   compounds in marine aerosols from the western North Pacific. Global Biogeochemical
874   Cycles 17, 3-1-3-19.

875 Kemp, E.M., 1975. Palynology of Leg 28 drill sites, Deep Sea Drilling Project. Initial Reports of the
876   Deep Sea Drilling Project 28, 599-623.

877 Kemp, E.M., Barrett, P. J., 1975. Antarctic glaciation and early Tertiary vegetation. Nature 258, 507-
878   508.

879 Kraus, C., 2016. Oligocene to early Miocene glacimarine sedimentation of the central Ross Sea, and
880   implications for the evolution of the West Antarctic Ice Sheet (Unpublished Masters Thesis).
881   Victoria University of Wellington, New Zealand.

882 Kvenvolden, K.A., Rapp, J.B., Golan-Bac, M., Hostettler, F.D., 1987. Multiple sources of alkanes in
883   Quaternary oceanic sediment of Antarctica. Organic geochemistry 11, 291-302.

884 Lehtonen, K., Ketola, M., 1993. Solvent-extractable lipids of Sphagnum, Carex, Bryales and Carex-

885   Bryales peats: content and compositional features vs peat humification. Organic

886   Geochemistry 20, 363-380.

887 Levy, R.H., Harwood, D.M., 2000. Tertiary marine palynomorphs from the McMurdo Sound erratics,

888   Antarctica. In Stilwel, J.D., Feldman, R.M. (Eds.), Paleobiology and Paleoenvironments of

889   Eocene Rocks: McMurdo Sound, East Antarctica, American Geophysical Union, Washington,

890   D.C., pp. 183-242.

891 Levy, R., Harwood, D., Florindo, F., Sangiorgi, F., Tripati, R., von Eynatten, H., Gasson, E., Kuhn.

892   G., Tripati, A., DeConto, R., Fielding, C., Field, B., Golledge, N., McKay, R., Naish, T., Olney,

893   M., Pollard, D., Schouten, S., Talarico, F., Warny, S., Willmott, V., Acton, G., Panter, K.,

894   Paulsen, T., Taviani, M., SMS Science Team, 2016. Antarctic ice sheet sensitivity to

895   atmospheric CO_2 variations in the early to mid-Miocene. Proceedings of the National Academy

896   of Sciences 113, 3453-3458.

897 Lewis, A.R., Marchant, D.R., Kowalewski, D.E., Baldwin, S.L., Webb, L.E., 2006. The age and

898   origin of the Labyrinth, western Dry Valleys, Antarctica: Evidence for extensive middle

899   Miocene subglacial floods and freshwater discharge to the Southern Ocean. Geology 34, 513-

900   516.

901 Lewis, A.R., Marchant, D.R., Ashworth, A.C., Hemming, S.R., Machlus, M.L., 2007. Major middle

902   Miocene global climate change: Evidence from East Antarctica and the Transantarctic

903   Mountains. Geological Society of America Bulletin 119, 1449-1461.

904 Lewis, A.R., Marchant, D.R., Ashworth, A.C., Hedenäs, L., Hemming, S.R, Johnson, J.V., Leng,

905   M.J., Machlus, M.L., Newton, A.E., Raine, J.I., Willenbring, J.K., Williams, M., Wolfe, A.P.,

906   2008. Mid-Miocene cooling and the extinction of tundra in continental Antarctica. Proceedings

907   of the National Academy of Sciences 105, 10676-10680.

908 Lewis, A.R., Ashworth, A.C., 2016. An early to middle Miocene record of ice-sheet and landscape

909   evolution from the Friis Hills, Antarctica. Geological Society of America Bulletin 128, 719-

910   738.

911 Luyendyk, B.P., Sorlien, C.C., Wilson, D.S., Bartek, L.R., Siddoway, C.S., 2001. Structural and

912   tectonic evolution of the Ross Sea rift in the Cape Colbeck region, Eastern Ross Sea,

913   Antarctica. Tectonics 20, 933-958.

914 Madureira, L.A., Piccinini, A., 1999. Lipids as indicators of paleoclimatic changes, II: terrestrial

915   biomarkers. Revista Brasileira de Oceanografia 47, 115-125.

916 Marchant, D.R., Denton, G.H., 1996. Miocene and Pliocene paleoclimate of the Dry Valleys region,

917   southern Victoria Land: a geomorphological approach. Marine Micropaleontology 27, 253-271.

918 Marchant, D.R., Denton, G.H., Swisher, C.C., Potter, N., 1996. Late Cenozoic Antarctic paleoclimate

919   reconstructed from volcanic ashes in the Dry Valleys region of southern Victoria

920   Land. Geological Society of America Bulletin 108, 181-194.

921   Martin, A.P., Cooper, A.F., Dunlap, W.J., 2010. Geochronology of Mount Morning, Antarctica: two-
922   phase evolution of a long-lived trachyte-basanite-phonolite eruptive center. Bulletin of
923   Volcanology 72, 357-371.

924   Matsumoto, G.I., Funaki, M., Machihara, T., Watanuki, K., 1986. Alkanes and alkanoic acids in the
925   Beacon Supergroup samples from the Allan Hills and the Carapace Nunatak in
926   Antarctica. Memoirs of National Institute of Polar Research. Special issue 43, 149-158.

927   Matsumoto, G. I., Machihara, T., Suzuki, N., Funaki, M., Watanuki, K., 1987. Steranes and
928   triterpanes in the Beacon Supergroup samples from southern Victoria Land in Antarctica.
929   Geochimica et Cosmochimica Acta 51, 2663-2671.

930   Matsumoto, G.I., Akiyama, M., Watanuki, K., Torii, T., 1990a. Unusual distributions of long-chain n-
931   alkanes and n-alkenes in Antarctic soil. Organic Geochemistry 15, 403-412.

932   Matsumoto, G. I., Hirai, A., Hirota, K., Watanuki, K., 1990b. Organic geochemistry of the McMurdo
933   dry valleys soil, Antarctica. Organic Geochemistry 16, 781-791.

934   Matsumoto, G.I., Honda, E., Sonoda, K., Yamamoto, S., Takemura, T., 2010. Geochemical features
935   and sources of hydrocarbons and fatty acids in soils from the McMurdo Dry Valleys in the
936   Antarctic. Polar Science 4, 187-196.

937   McKay, R., Browne, G., Carter, L., Cowan, E., Dunbar, G., Krissek, L., Naish, T., Powell, R., Reed,
938   J., Talarico, F., Wilch, T., 2009. The stratigraphic signature of the late Cenozoic Antarctic Ice
939   Sheets in the Ross Embayment. Geological Society of America Bulletin 121, 1537-1561.

940   McKay, R., Naish, T., Carter, L., Riesselman, C., Dunbar, R., Sjunneskog, C., Winter, D., Sangiorgi,
941   F., Warren, C., Pagini, M., Schouten, S., Willmott, V., Levy, R., DeConto R., Powell, R. D.,
942   2012. Antarctic and Southern Ocean influences on Late Pliocene global cooling. Proceedings of
943   the National Academy of Sciences 109, 6423-6428.

944   Mackenzie, A. S., Patience, R. L., Maxwell, J. R., Vandenbroucke, M., Durand, B., 1980. Molecular
945   parameters of maturation in the Toarcian shales, Paris Basin, France—I. Changes in the
946   configurations of acyclic isoprenoid alkanes, steranes and triterpanes. Geochimica et
947   Cosmochimica Acta 44, 1709-1721.

948   Meyers, P.A., Ishiwatari, R., 1993. Lacustrine organic geochemistry—an overview of indicators of
949   organic matter sources and diagenesis in lake sediments. Organic geochemistry 20, 867-900.

950   Mildenhall, D.C., 1989. Terrestrial palynology. In: Barrett, P.J. (Ed.), Antarctic Cenozoic history from
951   the CIROS-1 drillhole, McMurdo Sound. DSIR Publishing, Wellington, New Zealand, pp. 119-
952   127.

953   Miller, M.C., McCave, I.N., Komar, P., 1977. Threshold of sediment motion under unidirectional
954   currents. Sedimentology 24, 507-527.

955   Moossen, H., Bendle, J., Seki, O., Quillmann, U., Kawamura, K., 2015. North Atlantic Holocene
956   climate evolution recorded by high-resolution terrestrial and marine biomarker
957   records. Quaternary Science Reviews 129, 111-127.

958   Morin, R.H., Williams, T., Henrys, S.A., Magens, D., Niessen, F., Hansaraj, D., 2010. Heat flow and

959   hydrologic characteristics at the AND-1B borehole, ANDRILL McMurdo Ice Shelf Project,

960   Antarctica. Geosphere 6, 370-378.

961   Naish, T.R., Barrett, P.J., Dunbar, G.B., Woolfe, K.J., Dunn, A.G., Henrys, S.A., Claps, M., Powell,

962   R.D., Fielding, C.R., 2001. Sedimentary cyclicity in CRP drillcore, Victoria Land Basin,

963   Antarctica. Terra Antarctica 8, 225-244.

964   Naish, T., Powell, R., Levy, R., Wilson, G., Scherer, R., Talarico, F., Krissek, L., Niessen, F.,

965   Pompilio, M., Wilson, T., Carter, L., DeConto, R., Huybers, P., McKay, R., Pollard, D., Ross,

966   J., Winter, D., Barrett, P., Browne, G., Cody, R., Cowan, E., Crampton, J., Dunbar, G., Dunbar,

967   N., Florindo, F., Gebhardt, C., Graham, I., Hannah, M., Hansaraj, D., Harwood, D., Helling, D.,

968   Henrys, S., Hinnov, L., Kuhn, G., Kyle, P., Läufer, A., Maffioli, P., Magens, D., Mandernack,

969   K., McIntosh, W., Millan, C., Morin R., Ohneiser, C., Paulsen, T., Persico, D., Raine, I., Reed,

970   J., Riesselman, C., Sagnotti, L., Schmitt, D., Sjunneskog, C., Strong, P., Taviani, M., Vogel, S.,

971   Wilch T., Williams, T., 2009. Obliquity-paced Pliocene West Antarctic ice sheet oscillation.

972   Nature 458, 322-328.

973   Ourisson, G., Albrecht, P., 1992. Hopanoids. 1. Geohopanoids: the most abundant natural products on

974   Earth? Accounts of Chemical Research 25, 398-402.

975   Peters, K. E., Moldowan, J. M., 1991. Effects of source, thermal maturity, and biodegradation on the

976   distribution and isomerization of homohopanes in petroleum. Organic geochemistry 17, 47-61.

977   Pole, M., Hill, B., Harwood, D., 2000. Eocene plant macrofossils from erratics, McMurdo Sound,

978   Antarctica. In: Stilwel, J.D., Feldman, R.M. (Eds.), Paleobiology and Paleoenvironments of

979   Eocene Rocks: McMurdo Sound, East Antarctica, American Geophysical Union, Washington,

980   D.C., pp. 243-251.

981   Powell, R., Krissek, L.A., Van der Meer, J., 2000. Preliminary depositional environmental analysis of

982   CRP-2/2A, Victoria Land Basin, Antarctica: palaeoglaciological and palaeoclimatic

983   inferences. Terra Antarctica 7, 313-322.

984   Powell, R.D., Cooper, J.M., 2002. A glacial sequence stratigraphic model for temperate, glaciated

985   continental shelves. Geological Society, London, Special Publications 203, 215-244.

986   Powell, R.D., Domack, E.W., 2002. Modern glacimarine environments. In: Menzies, J. (Ed.), Modern

987   and Past Glacial Environments, Butterworth-Heinemann, Boston, pp. 361-390.

988   Poynter, J.G., Farrimond, P., Robinson, N., Eglinton, G., 1989. Aeolian-derived higher plant lipids in

989   the marine sedimentary record: Links with palaeoclimate. In: Leinen, M., Sarnthein, M.,

990   (Eds.), Paleoclimatology and paleometeorology: modern and past patterns of global

991   atmospheric transport, Springer, Netherlands, pp. 435-462

992   Prebble, J.G., Raine, J.I., Barrett, P.J., Hannah, M.J., 2006a. Vegetation and climate from two

993   Oligocene glacioeustatic sedimentary cycles (31 and 24 Ma) cored by the Cape Roberts Project,

994   Victoria Land Basin, Antarctica. Palaeogeography, Palaeoclimatology, Palaeoecology 23, 41-
995   57.

996   Prebble, J.G., Hannah, M.J., Barrett, P.J., 2006b. Changing Oligocene climate recorded by
997   palynomorphs from two glacio-eustatic sedimentary cycles, Cape Roberts Project, Victoria
998   Land Basin, Antarctica. Palaeogeography, Palaeoclimatology, Palaeoecology 231, 58-70.

999   Pross, J., Contreras, L., Bijl, P.K., Greenwood, D. R., Bohaty, S.M., Schouten, S., Bendle, J.A., Röhl,
1000   U., Tauxe, L., Raine, J.I., Huck, C.E., van de Flierdt, T., Jamieson, S.S.R., Stickley, C.E., van
1001   de Scootbrugge, B., Escutia, C., Brinkhuis, H., Integrated Ocean Drilling Program Expedition
1002   318 Scientists, 2012. Persistent near-tropical warmth on the Antarctic continent during the early
1003   Eocene epoch. Nature 488, 73-77.

1004   Rees-Owen, R.L., Gill, F.L., Newton, R.J., Ivanović, R.F., Francis, J.E., Riding, J.B., Vane, C.H., dos
1005   Santos, R.A.L., 2018. The last forests on Antarctica: Reconstructing flora and temperature from
1006   the Neogene Sirius Group, Transantarctic Mountains. Organic Geochemistry
1007   doi.org/10.1016/j.orggeochem.2018.01.001.

1008   Ribecai, C., 2007. Early Jurassic miospores from Ferrar Group of Carapace Nunatak, South Victoria
1009   Land, Antarctica. Review of Palaeobotany and Palynology 144, 3-12.

1010   Rohmer, M., Bouvier-Nave, P., Ourisson, G., 1984. Distribution of hopanoid triterpenes in
1011   prokaryotes. Microbiology 130, 1137-1150.

1012   Sachse, D., Radke, J., Gleixner, G., 2006. δD values of individual n-alkanes from terrestrial plants
1013   along a climatic gradient–Implications for the sedimentary biomarker record. Organic
1014   Geochemistry 37, 469-483.

1015   Sackett, W.M., Poag, C.W., Eadie, B.J., 1974. Kerogen recycling in the Ross Sea,
1016   Antarctica. Science 185, 1045-1047.

1017   Sandroni, S., Talarico, F., 2004. Petrography and provenance of basement clasts in CIROS-1 core,
1018   McMurdo Sound, Antarctica. Terra Antarctica 11, 93-114.

1019   Sandroni, S., Talarico, F.M., 2011. The record of Miocene climatic events in AND-2A drill core
1020   (Antarctica): Insights from provenance analyses of basement clasts. Global and Planetary
1021   Change 75, 31-46.

1022   Schefuß, E., Ratmeyer, V., Stuut, J.B.W., Jansen, J.H.F., Sinninghe Damsté, J.S., 2003. Carbon
1023   isotope analyses of n-alkanes in dust from the lower atmosphere over the central eastern
1024   Atlantic. Geochimica et Cosmochimica Acta 67, 1757-1767.

1025   Schellekens, J., Buurman, P., Pontevedra-Pombal, X., 2009. Selecting parameters for the
1026   environmental interpretation of peat molecular chemistry–a pyrolysis-GC/MS study. Organic
1027   Geochemistry 40, 678-691.

1028   Schellekens, J., Buurman, P., 2011. n-Alkane distributions as palaeoclimatic proxies in ombrotrophic
1029   peat: the role of decomposition and dominant vegetation. Geoderma 164, 112-121.

1030 Scherer, R., Hannah, M., Maffioli, P., Persico, D., Sjunneskog, C., Strong, C. P., Taviani, M., Winter,
1031   D., 2007. Palaeontologic characterisation and analysis of the AND-1B core, ANDRILL
1032   McMurdo Ice Shelf Project, Antarctica. Terra Antarctica 14, 223-254.

1033 Schröder, H., Paulsen, T., Wonik, T., 2011. Thermal properties of the AND-2A borehole in the
1034   southern Victoria Land Basin, McMurdo Sound, Antarctica. Geosphere 7, 1324-1330.

1035 Seifert, W. K., Moldowan, J. M., 1978. Applications of steranes, terpanes and monoaromatics to the
1036   maturation, migration and source of crude oils. Geochimica et Cosmochimica Acta 42, 77-95.

1037 Seifert, W. K., Moldowan, J. M., 1980. The effect of thermal stress on source-rock quality as
1038   measured by hopane stereochemistry. Physics and Chemistry of the Earth 12, 229-237.

1039 Shackleton, N.J., Kennett, J.P., 1975. Paleotemperature history of the Cenozoic and the initiation of
1040   Antarctic glaciation: oxygen and carbon isotope analyses in DSDP Sites 277, 279, and
1041   281. Initial reports of the deep sea drilling project 29, 743-755.

1042 Smellie, J.L., 2001. History of Oligocene erosion, uplift and unroofing of the Transantarctic
1043   Mountains deduced from sandstone detrital modes in CRP-3 drillcore, Victoria Land Basin,
1044   Antarctica. Terra Antarctica 8, 481-490.

1045 Strogen, D.P., Bland, K.J., 2011. Hydrocarbon Risk for Drilling on the Coulman High, GNS Science
1046   Consultancy Report Volume 2011/185, GNS Science, Lower Hutt, New Zealand.

1047 Strong, C. P., Webb, P. N., 2000. Oligocene and Miocene Foraminifera from CRP-2/2A, Victoria
1048   Land Basin, Antarctica. Terra Antarctica 7, 461-472.

1049 Sugden, D.E., Marchant, D.R., Denton, G.H., 1993. The case for a stable East Antarctic ice sheet: the
1050   background. Geografiska Annaler. Series A. Physical Geography 75, 151-154.

1051 Sugden, D., Denton, G., 2004. Cenozoic landscape evolution of the Convoy Range to Mackay Glacier
1052   area, Transantarctic Mountains: onshore to offshore synthesis. Geological Society of America
1053   Bulletin 116, 840-857.

1054 Talarico, F., Sandroni, S., Fielding, C. R., Atkins, C., 2000. Variability, petrography and provenance
1055   of basement clasts in core from CRP-2/2A, Victoria Land Basin, Antarctica. Terra Antarctica 7,
1056   529-544.

1057 Talbot, H. M., Farrimond, P., 2007. Bacterial populations recorded in diverse sedimentary
1058   biohopanoid distributions. Organic Geochemistry 38, 1212-1225.

1059 The Shipboard Scientific Party, 1975a. Shipboard Site Reports: Sites 270, 271, 272. Initial Reports of
1060   the Deep Sea Drilling Project 28, 211-334.

1061 The Shipboard Scientific Party, 1975b. Shipboard Site Reports: Site 274. Initial Reports of the Deep
1062   Sea Drilling Project 28, 369-433.

1063 Tissot, B.P., Welte, D.H., 1984. Petroleum Formation and Occurrence (2nd ed.). Springer-Verlag,
1064   Berlin Heidelberg.

1065 Truswell, E.M., Drewry, D.J., 1984. Distribution and provenance of recycled palynomorphs in
1066   surficial sediments of the Ross Sea, Antarctica. Marine Geology 59, 187-214.

1067 Venkatesan, M.I., 1988. Organic geochemistry of marine sediments in Antarctic region: marine lipids
1068   in McMurdo Sound. Organic Geochemistry 12, 13-27.

1069 Vogts, A., Moossen, H., Rommerskirchen, F., Rullkötter, J., 2009. Distribution patterns and stable
1070   carbon isotopic composition of alkanes and alkan-1-ols from plant waxes of African rain forest
1071   and savanna C_3 species. Organic Geochemistry 40, 1037-1054.

1072 Warny, S., Askin, R.A., Hannah, M.J., Mohr, B.A., Raine, J.I., Harwood, D.M., Florindo, F., 2009.
1073   Palynomorphs from a sediment core reveal a sudden remarkably warm Antarctica during the
1074   middle Miocene. Geology 37, 955-958.

1075 Webb, P.N., Harwood, D.M., McKelvey, B.C., Mercer, J.H., Stott, L.D., 1984. Cenozoic marine
1076   sedimentation and ice-volume variation on the East Antarctic craton. Geology 12, 287-291.

1077 Whittaker, J.M., Müller, R.D., 2006. Seismic stratigraphy of the Adare Trough area,
1078   Antarctica. Marine geology 230, 179-197.

1079 Wilson, D.S., Luyendyk, B.P., 2009. West Antarctic paleotopography estimated at the Eocene-
1080   Oligocene climate transition. Geophysical Research Letters 36, L16302,
1081   doi:10.1029/2009GL039297.

1082 Zhou, W., Xie, S., Meyers, P.A., Zheng, Y., 2005. Reconstruction of late glacial and Holocene
1083   climate evolution in southern China from geolipids and pollen in the Dingnan peat
1084   sequence. Organic Geochemistry 36, 1272-1284.